GLASS FORMING ABILITY AND RELAXATION BEHAVIOUR OF Zr BASED METALLIC GLASSES

A Thesis

by

ARAVIND MIYAR KAMATH

Submitted to the Office of Graduate Studies of
Texas A&M University
in partial fulfillment of the requirements for the degree of

MASTER OF SCIENCE

May 2011

Major Subject: Mechanical Engineering

Glass Forming Ability and Relaxation Behaviour of Zr Based Metallic Glasses

GLASS FORMING ABILITY AND RELAXATION BEHAVIOUR OF Zr BASED METALLIC GLASSES

A Thesis

by

ARAVIND MIYAR KAMATH

Submitted to the Office of Graduate Studies of
Texas A&M University
in partial fulfillment of the requirements for the degree of

MASTER OF SCIENCE

Approved by:

Chair of Committee,	Jorge Alvarado
Committee Members,	Xinghang Zhang
	Alex Fang
Head of Department,	Dennis C. O'Neal

May 2011

Major Subject: Mechanical Engineering

ABSTRACT

Glass Forming Ability and Relaxation Behavior of Zr Based Metallic Glasses.

(May 2011)

Aravind Miyar Kamath, B.E., Manipal Institute of Technology

Chair of Advisory Committee: Dr. Jorge Alvarado

Metallic glasses can be considered for many commercial applications because of the higher mechanical strength, corrosion and wear resistance when compared to crystalline materials. To consider them for novel applications, the challenge of preparing metallic glasses from the liquid melt phase and how the properties of metallic glasses change due to relaxation need to be understood better. The glass forming ability (GFA) with variation in composition and inclusion of different alloying elements was studied by using thermal techniques to determine important GFA indicators for Zr-based bulk metallic glasses (BMG). The effect of alloying elements, annealing temperature and annealing time on the thermal and structural relaxation of the BMGs was studied by using an annealing induced relaxation approach. The thermal relaxation was studied by measuring specific heat of the samples using differential scanning calorimeter (DSC) and calculating the enthalpy recovery on reheating in the BMG samples. The structural relaxation was also studied by using extended X-ray absorption fine structure (EXAFS) technique on the as-obtained and relaxed samples. The effects of alloying elements and annealing on electrical resistance were studied by using a two point probe.

From the study, it was found that the currently used GFA indicators are inadequate to fully capture and identify the best GFA BMGs. The fragility (β) of the melt is a new criterion that has been proposed to measure and analyze GFA. The enthalpy relaxation of Zr-based BMGs was found to follow a stretched exponential function, and the parameters obtained showed the BMGs used in the current study are strong glass formers. EXAFS studies showed variations in the structure of BMGs with changes in alloying elements. Furthermore, alloying elements were found to have an effect on the structure of the relaxed BMGs. The resistance of BMGs was found to decrease with relaxation which can be attributed to short range order on annealing.

ACKNOWLEDGEMENTS

This work would be incomplete without thanking all the people who helped me accomplish it. First, I express my sincere gratitude to my advisor, Dr. Jorge Alvarado, for his guidance and support throughout my Master's program. Next I thank Dr. Charles Marsh , Dr. Carl Feickert and Nick Hinton at the US Army Corps of Engineers for their support and knowledge sharing in the area of metallic glasses. Also I thank my committee members, Dr. Xinghang Zhang of the Department of Mechanical Engineering and Dr. Alex Fang of the Department of Engineering Technology and Industrial Distribution at Texas A & M University, for their valuable input. A special mention has to be made of Dr. Abraham Clearfield, Dr. Raymundo Arroyave, and Dr. Tahir Cagin, who made time in their busy schedule to share their knowledge in this field.

Next, I want to make a mention of all those people without whom I would have been unable to conduct this study. These include: Dr. Tom Shen at NanoAmor for the samples, Dr. Bhuvanesh for XRD testing, Mr. Bill Merkwa at the glass shop, Dr. Dmitri Lagoudas/Rodney Inmon for the DSC facility, Dr. Kalyan Annamalai/Ben Lawrence for the TGA facility, Mr. Mark Stauffer/Dr. Frank Huggins for the EXAFS analysis, and Dr. Lin Shao for the two point probe. Also I thank my research team members: Guillermo Soriano, Shreyas Bhimani and Clark Maxfield and the Engineering Technology and Industrial Distribution staff for helping me in my experimental work.

Finally, I owe a big thanks to my family and friends without whom I would not have been able to endure through this program for which I am grateful to them.

TABLE OF CONTENTS

CHAPTER Page

LIST OF FIGURES

FIGURE Page

FIGURE Page

FIGURE Page

FIGURE Page

LIST OF TABLES

CHAPTER I

INTRODUCTION

Amorphous metals or glassy metals as they are called do not have a defined long range structure and as a result they tend to be isotropic like liquids and gases. They tend to have a disordered arrangement of atoms, where we can see a short range order but not a uniform long range order as in a crystal structure. They can be obtained for any metallic system provided the melt is quenched at a rate that is fast enough to prevent nuclei formation and crystal growth [1]. The first metallic glass obtained was an alloy of Au_3Si in 1960 by Klement, Willens, and Duwez [2]. The cooling rates had to be of the order of 10^6 K/s [3]. The high cooling rate arrest or suppress nucleation and freezes the atoms in a random order leading to an amorphous structure.

There are different methods for preparing amorphous solids from solids, liquids or gases as illustrated by Fig.1. They can be obtained from crystalline solids by mechanical processing, irradiation and shock waves. Thermal evaporation under vacuum, cathode sputtering and chemical vapor deposition are some of the methods that are used to form amorphous solids from gases.

In most research studies, amorphous solids are obtained from the liquid melt by using high cooling rates. Several techniques have been developed to achieve these cooling rates. Duwez et al. [2, 4] proposed the splat-quenching or the gun technique that

---

This thesis follows the style of Acta Materialia.

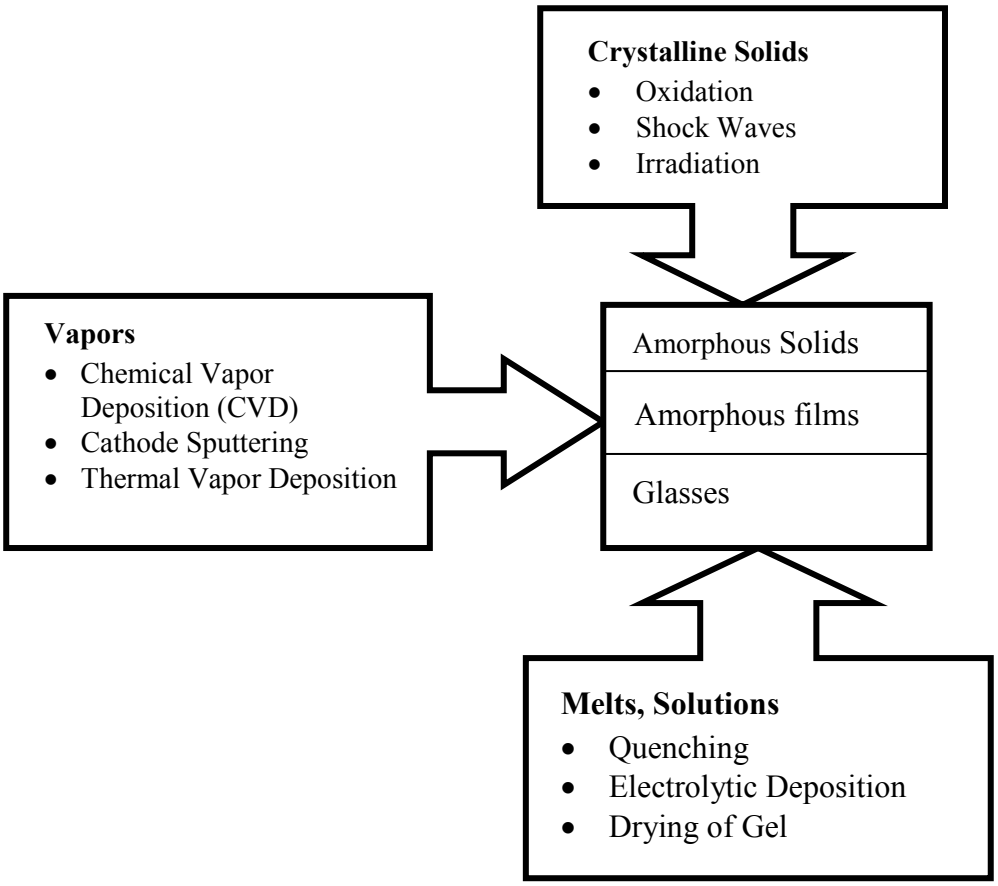

FIG.1 Schematic of paths of formation of amorphous solids[2]

propagates a shock wave in a vacuum that hits the melt and forces it through a small opening on to a cooler substrate. Another method is called the piston-and-anvil method [2, 4] where the melt is pressed between a reciprocating piston and a stationary anvil that converts the melt drops to thin layers forming an amorphous structure. Other techniques like centrifugal spinning and jet spinning have also been used to obtain metallic glasses from the melt solution. The most common technique that has been used by researchers to obtain metallic glasses is the melt spinning technique that allows producing continuous

ribbons from the melt solution. In this method the melt is pressurized through a nozzle and drops on to a rotating disc or cylinder that is maintained at a cooler temperature and quenches the melt at fast rates [2]. Continuous ribbons are produced by melt spinning that have a characteristic thickness of a few microns.

The amorphous structure formed by rapid cooling has some short range order at the atomic level. However, as the distance from this short range order increases the structural configurations vary rapidly with different bond lengths and bond angles [2]. This variation in structure when compared to a crystal of similar composition imparts certain superior physical properties to amorphous materials. The absence of grain boundaries and dislocations in the amorphous material results in a uniform structure that leads to higher strength, hardness, wear resistance and corrosion resistance [5].

CHAPTER II

LITERATURE REVIEW

One of the major challenges for using metallic glasses in commercial applications has been the difficulty in making them from the liquid melt. Metallic glasses require very high cooling rates of the order of 10^5-10^6 K/s. Such a high rate of cooling suppresses crystal growth resulting in a crystal percentage between 0.1% and .0001% [6]. The required cooling rates have limited the number of alloy systems that could form metallic glasses. Furthermore, metallic glasses can only be made consistently if the thickness of the material is on the order of microns [3]. With the discovery of bulk metallic glasses (BMG) in 1990 which consist of three or more metallic components, metallic glasses could be obtained at much lower cooling rates of the order of 100 K/s and even lower [3]. Bulk metallic alloys have been prepared in numerous multi-component alloy systems with elemental groups that include Mg, Zr and Ti, Fe, Pd, Ni and Cu [7] .

Fig.2 schematically shows the relative magnitude of cooling rates required to form metallic glasses and BMGs from their corresponding liquid melt. T_m and T_g correspond to the melting point and glass transition temperature. It can be easily understood that BMGs require much lower cooling rates to avoid any intersection with the time temperature transformation (TTT) curve when compared to metallic glasses. As a result of the much lower cooling rates required for BMGs, alloys of much greater volume (diameter or thickness) have been produced in the last decade. BMGs exhibit

good thermal stability and a wide supercooled liquid region, making it possible to measure its thermodynamic properties over a wide temperature range [8].

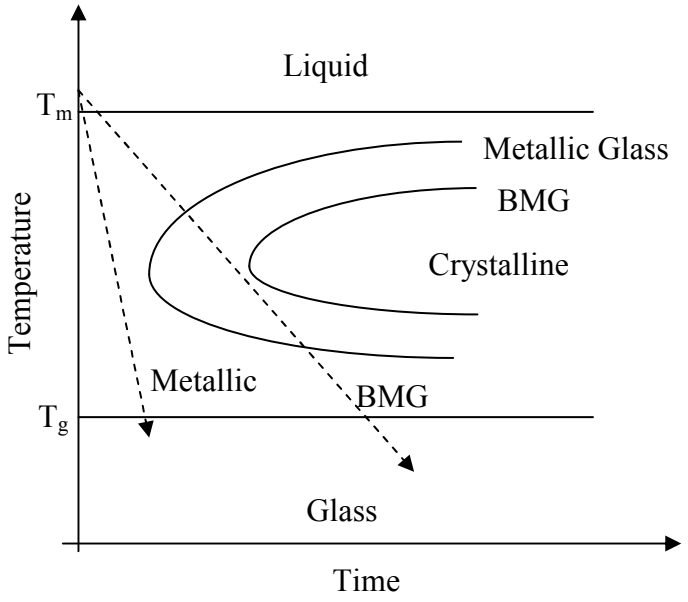

FIG.2 Schematic time-temperature-transition diagram of glass formation from melt [3]

2.1 Glass Forming Ability (GFA)

Inoue [9] defined three empirical rules that have to be satisfied to form a BMG alloy. These are: a) they need to be formed of three or more elements, b) a significant difference in atomic size ratio of 12% or more between the main three constituent elements, and c) a high negative heat of mixing between the three main constituent elements. Although these rules are useful in developing novel systems of metallic glasses, obtaining glasses from melts continues to remain a challenge. A lot of effort has been focused on understanding the factors that govern the glass forming ability of different metallic systems. Glass forming ability (GFA) is a metric used to quantify the

ease with which a metallic glass can be obtained from a liquid melt. This parameter can be directly assessed by noting the critical cooling rate required to make BMG. Also, critical size obtained for a particular alloy system has been used as a GFA indicator. The critical cooling rate is the lowest cooling rate required for forming a glass of a particular size. In other words, GFA improves when the critical cooling rate decreases or critical size increases for an alloy system. However, the critical cooling rate is difficult to measure accurately from experiments and the maximum attainable size is difficult to quantify as it varies based on the method used to manufacture metallic glasses. As a result, various researchers have attempted to study GFA by analyzing the underlying mechanisms involved in these systems and came up with physical mechanisms like structural models, free electron theory, chemical factors like bond strength and electronegativity, phase diagram features and atomic size criterion to name a few to quantify GFA of a system. However, these approaches considered only structural and thermodynamic factors while kinetics of the glass formation like nucleation and crystal growth were ignored [10]. Researchers then attempted to study the glass forming ability of different alloying systems considering kinetics and came up with parameters describing the glass stability on heating. These parameters have shown to play an important role in development of new compositions of metallic glasses.

Turnbull [11] considered nucleation frequency and came up with the reduced glass transition temperature parameter to compare GFA between different alloy system. Among the many GFA parameters, the reduced glass transition temperature T_{rg} defined as the ratio of the glass transition temperature (T_g) to the liquidus temperature (T_l) is one

commonly used. Turnbull and Fisher [12] stated that the value of T_{rg} approaches 0.66 for good glass formers regardless of the composition of the glass forming system. Weinberg [6] proposed the ratio of the difference in peak crystallization temperature (T_x^h) and glass transition temperature (T_g) to the melting point of the alloy (T_m) , $\frac{T_x^h - T_g}{T_m}$. Other researchers like Hruby [6] proposed parameters based on the assumption that GFA of a system is higher if it has higher stability against crystallization. Another good GFA parameter proposed by Angell [6] was the difference in temperature between peak crystallization temperature (T_x^h) and glass transition temperature (T_g). Of all the parameters, $\gamma = \frac{T_x}{T_g + T_l}$ where T_x corresponds to crystallization temperature, T_g is the glass transition temperature and T_l is the liquidus temperature proposed by Lu and Liu [13] has been found to be the most reliable indicator. It is found to have a good correlation with the critical cooling rate over a range of alloying systems.

At this stage it is important to analyze the reliability of the γ-indicator and the factors that were considered while deriving this parameter. When studying GFA, two critical components that need to be considered are the liquid phase stability and resistance to crystallization in the alloy system considered. While the former depends on the short range chemical and structural ordering of the atoms in the melt and its thermodynamic stability, the latter depends on the stability of the amorphous phase with respect to the crystalline phase, and the kinetic stability related to nucleation and crystal growth. In other words, the longer the system can stay as a liquid when cooling without

allowing crystal nucleation and growth, the better the GFA of the system is. The liquid phase stability comprises of two main features: the stability of the liquid when in equilibrium, that is, before reaching the melting point (T_l) of the system, and the stability of the supercooled liquid between the melting point and the glass transition temperature. If we consider two systems that have the same T_g but different T_l, the one with the lower T_l value is considered to have higher liquid stability. In the same manner, if two systems have same T_l and different T_g, the system with the lower T_g is more stable in the supercooled state. When the system have different T_l and T_g, the average of T_l and T_g are considered when analyzing stability. In general, the system having a lower $\frac{T_g + T_l}{2}$ is considered to have higher liquid stability [10].

The second component when studying GFA is resistance to crystallization. In general, when metallic glasses are heated, they tend to start crystallizing at some temperature (T_x) which lies beyond the T_g of the system. If we assume the liquid stability is the same for different systems, then T_x will be the defining factor to determine GFA. The system that has a higher T_x can be considered to be having a higher resistance to crystallization. When the liquid stability and crystallization are considered together, GFA of a system can be expressed as being proportional to the term $T_x\left[\frac{1}{2(T_g + T_l)}\right]$ or $\frac{\gamma}{2}$. The term γ was derived from this expression as $\gamma = \frac{T_x}{T_g + T_l}$ [10].

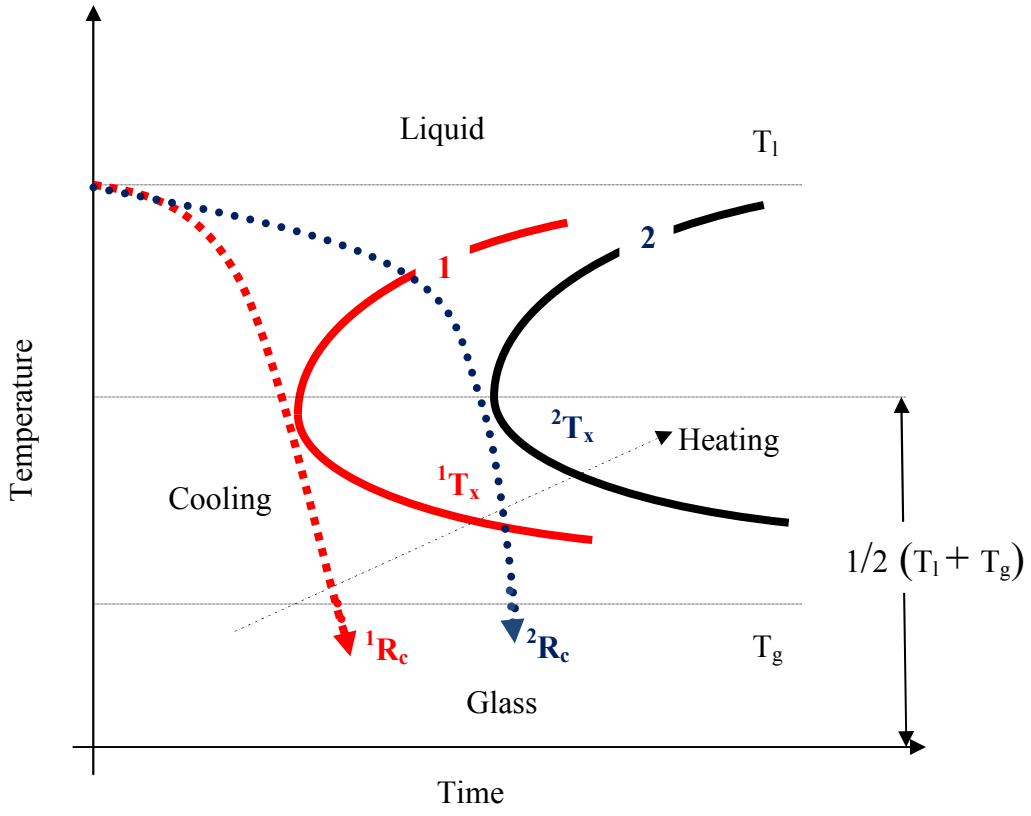

FIG.3 Schematic time-temperature transition diagram showing effect of T_x [10]

Fig.3 illustrates the effect of T_x on the GFA of a system. If we consider the systems 1 and 2 having same values for T_g and T_l, then liquid phase stability as explained before will be inversely proportional to the average of T_g and T_l. Since the values of T_g and T_l are equal for both systems, the liquid phase stability is the same for them. As seen in the figure, system 2 has a higher T_x on heating than system 1. If we compare the critical cooling rate R_c for the two systems, we see that ^2R_c is less than ^1R_c. In other words system 2 can be transformed into a glass more easily from the liquid melt than system 1. From this, it is clear that a higher T_x leads to a higher GFA for a system.

The parameter γ has been analyzed for a range of alloying systems and found to have a very good correlation with the critical cooling rate, making it one of the more reliable GFA indicators [10].

2.2 Relaxation

It has been observed that properties of BMGs or glasses in general undergo changes over a period of time. These property changes have been attributed to the transition from metastable configuration to near-equilibrium state. BMGs tend to be metastable because of the excess energy contained in the system during glass forming from a liquid melt. Glass forming requires high cooling rates and as a result the liquid melt continues to exist as a supercooled liquid beyond the melting point (T_m) until it reaches the glass transition temperature (T_g) as shown in Fig.4. T_g is widely defined as the temperature at which the viscosity is 10^{13} poise or greater [2, 14].

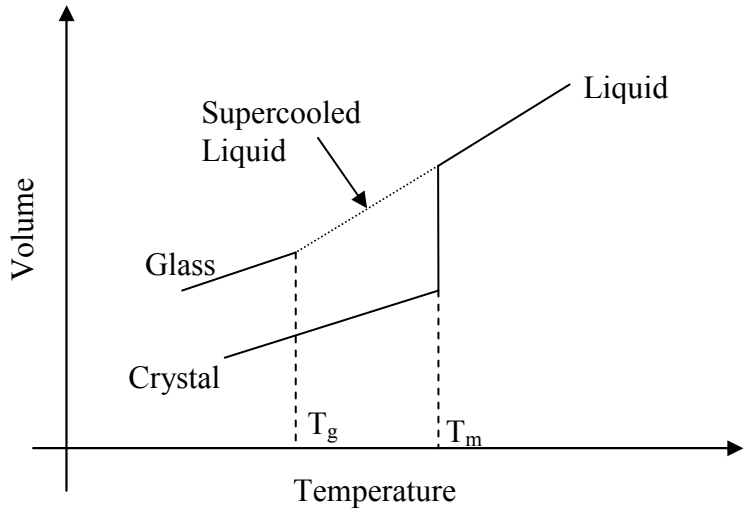

FIG.4 Schematic of glass formation from liquid melt [1, 15]

Fig.4 shows the formation of a glass from the liquid melt. In the supercooled state, the liquid continues to maintain quasi-equilibrium (metastable state) for some time. During this time period, thermal properties like enthalpy and entropy maintain their values despite the high cooling rate. The number and type of bonds among atoms, and their translational and vibrational behavior continue to change with temperature; however as the cooling proceeds, these thermal and structural parameters can no longer keep pace with the high cooling rate. As a result, the amount of enthalpy that is remaining in the liquid phase exceeds the equilibrium value of the system at the given temperature. The supercooled liquid system is now considered to be in a metastable state and continues to be in this state even when it freezes into a disordered structure at the glass transition temperature [2]. The system has excess free energy in terms of the heat capacity when compared to the equilibrium state at the same temperature [16]. As a result, BMGs have a tendency to lose their free energy and move towards equilibrium over long periods of time. As this process proceeds towards equilibrium, there are changes in the physical and thermal properties of the material. The changes in the material properties with time are due to physical ageing, while the changes in thermal properties like heat capacity, entropy are due to enthalpy relaxation [17].

The time required to undergo relaxation increases with decreasing temperature. Also the temperature at which the glass transition occurs has been found to be a function of the cooling rate. Glasses with similar composition can show variations in structural and thermal properties as a result of different thermal histories [2]. From this discussion, it has become clear that the properties of metallic glasses depend on the way they are

produced. Furthermore, BMG properties tend to vary because of transformations that occur in these systems due to relaxation and aging.

While the process of relaxation occurs over an extended period of time, relaxation in BMGs can be studied by annealing the samples isothermally at temperatures below the glass transition. Since BMGs exhibit high thermal stability and wide supercooled liquid range, they do not undergo crystallization and phase separation when they are annealed close to T_g for long periods of time, making it possible to study relaxation. When the samples are annealed isothermally, they relax into their equilibrium supercooled liquid state leading to a decrease in enthalpy, entropy and volume of the system [8]. When annealed samples are reheated, previous studies have shown that BMGs have a tendency to recover the enthalpy and entropy lost during annealing [12], and other properties like thermal diffusivity, plasticity and electrical resistivity also change [18]. The thermal process of enthalpy recovery shows up as an endothermic peak on a differential scanning calorimeter thermograph which shows up below the glass transition temperature or as an overshoot at the upper edge of the glass transition [16, 19] temperature profile.

Inoue et al. [19] studied relaxation in a range of systems including Zr-Cu-, Al- and Fe-based systems. The study focused on understanding the enthalpy relaxation behavior in these systems. Differences in relaxation mechanisms were observed depending on the inclusion of metal or metalloid atoms in the composition. It was observed that many systems that constituted of metalloid elements like Fe-Ni-B and Fe-Ni-P systems showed two distinct stages during relaxation [20] , which was in contrast

with systems containing only metal elements. The metal-metalloid systems showed a two-stage structural relaxation behavior with one broad endothermic peak occurring above the annealing temperature, which is routinely called the low temperature peak. The second stage of relaxation consisted of an exothermic peak just below T_g . It was further stated that while the broad endothermic peak was reversible, the exothermic peak near T_g was irreversible. The reversible and irreversible peaks were attributed to the metal-metal and metal-metalloid bonds in these systems. The activation energy required for the second-stage of relaxation (high temperature peak) found using Kissinger analysis [20] was found to be higher than the first-stage of relaxation (low temperature peak). From these studies, it was concluded that the low temperature peak was due to local and medium range rearrangement of metal atoms while the second stage peak was due to the long range cooperative rearrangement of metal and metalloid atoms [20].

Recent studies regarding relaxation have been more focused on understanding the kinetics of isothermal relaxation to establish a function that would describe structural relaxation better in BMGs. There are different models that have been developed to explain relaxation in BMGs like the flow defect model, stretched exponential relaxation model, and the Sestak-Berggren SB kinetic model [18]. Current studies have involved understanding changes in enthalpy or other properties like volume or viscosity [21] with isothermal annealing. Formulation and analysis of the mathematical functions that would best describe the property changes with annealing have been proposed. Hahn [18] studied Zr-based, while Fan et al. [8] and Zhang et al. [22] studied Pd-based and La-based quaternary alloys for enthalpy relaxation, respectively. In these studies, the

samples were annealed at different temperatures below T_g for different periods of time and then scanned using a differential scanning calorimeter (DSC) to measure variations in heat flow with annealing. The enthalpy recovery derived from the DSC thermographs has been found to increase with increasing annealing time and found to fit a stretched exponential relaxation function: $\Delta H_T(t_a) = \Delta H_T(\infty)\{1 - \exp[-(\frac{t_a}{\tau})^{\beta}]\}$ where $\Delta H_T(\infty)$ is the equilibrium value of $\Delta H_T(t_a)$ for $t_a \to \infty$ at the annealing temperature T_a, τ is the relaxation time constant and β is the Kohlrausch exponent that has a value between 0 and 1. The values of $\Delta H_T(\infty)$ and τ are found to increase with decreasing annealing temperature in these studies. Both parameters appear to increase with decreasing annealing temperature because the atomic mobility required to achieve thermodynamic equilibrium is higher at higher temperatures. The value of β has been related to the degree of disorder of the supercooled liquid and used to find out whether the system is a strong or fragile supercooled liquid [22]. The concept of strong and fragile liquids evolved from the Angell plot [23]. The Angell plot is obtained by plotting the logarithm of viscosity as a function of T_g/T. The slope of the curve (m) is used to indicate how strong and fragile a metallic glass is. Strong glass forming liquids exhibit have a low m value while fragile glass formers usually have a relatively high m value.

Efforts have also been made by researchers to study the effects of relaxation on BMG structure when they are annealed below the glass transition temperature. Various techniques like X-ray diffraction, neutron diffraction and extended X-ray absorption fine structures (EXAFS) have been used to study the structure of BMGs before and after

annealing to observe changes that occur at the atomic level with annealing. Dmowski et al. [24] annealed samples of Vit 105 ($Zr_{52.5}Cu_{17.9}Ni_{14.6}Al_{10.0}Ti_{5.0}$) at approximately 50 K below T_g for different periods of time and probed the as-obtained and annealed samples using neutron diffraction. Pair-distribution functions of the resultant data indicated variations in the short and long inter-atomic distances while the density of the average inter-atomic distance increased. The authors of the study concluded that the variations in inter-atomic distances due to anneal-induced relaxation cannot be explained in terms of annihilation of the free volume because free volume annihilation should have led to only changes in the long inter-atomic distances. Yavari et al.[25] studied relaxation in Pd-based glass by *in-situ* heating using a X-ray diffraction technique and found changes in free volume of about 0.2% between the as-quenched and relaxed samples. Guoqiang et al.[26] studied structural relaxation in $Mg_{65}Cu_{25}Gd_{10}$ glass using EXAFS technique and found an increase in the short range order around Cu atoms with annealing leading to an increase in the coordination number of Cu. The short range order around Gd atoms was found to initially decrease and then increase with an increase in annealing time.

The effects of relaxation on mechanical properties like the Young's modulus and hardness [27] have been reported. Electrical properties such as resistivity have been found to change when annealed at different conditions. The resistivities of metallic glasses have been found to be as low as 30 μΩ-cm in Ag-Cu-Mg alloys to as high as 400 μΩ-cm in certain Ca-Al glasses. Temperature dependent resistivity of metallic glasses has been found to vary with the magnitude of the resistivity. Electrical resistivity in BMGs has been found to increase with increasing temperature in low resistivity alloys

while it has been found to decrease with temperature for high resistivity alloys [28]. With respect to annealing time, Kokmeijer et al. [29] found that the resistivity in $Fe_{40}Ni_{40}B_{20}$ decreases with annealing time, which could be attributed to changes in the short range ordering and reduction in free volume. Bai et al. [30] conducted a similar study on $Zr_{48}Nb_8Cu_{12}Fe_8Be_{24}$ and found a reduction in resistance with increasing annealing temperature below T_g. The negative temperature dependence of the resistivity was explained by assuming the system behaves like a liquid on heating and applying Ziman theory.

There are different competing theories that attempt to explain the reasons for relaxation in glasses. The two most significant theories are the Adam and Gibbs theory and the Free volume theory. The Adam and Gibbs theory [23] basically draws a relation between relaxation and thermodynamic quantities. It states that for atoms to move at low temperature, a cooperative movement of a group of atoms is required. According to this theory, relaxation occurs as a result of a sequence of individual movements where a sub-region of a system relaxes to a new configuration. The collective movement of the atoms is initiated as a result of an enthalpy fluctuation. The subsystem that undergoes this movement is called as a cooperatively rearranging region (CRR). The sub-region that has the smallest possible cooperatively rearranging possibility when compared to the larger regions tends to dominate the relaxation phenomenon. The drawback of the theory is that it cannot quantify the size of the rearranging sub-region and the number of atoms they contain among other variables. The theory predicts that relaxation is related to the cooperative motion of atoms, which increases with decreasing temperature.

Cohen and Turnbull [23] proposed the free volume theory to explain relaxation. This theory linked relaxation to the motion of atoms in the system. The theory states that the motion of atoms occurs only if there are vacant spaces available. If an atom is surrounded by neighboring atoms such that they form a cage-like structure, then the movement of the atom is restricted and it cannot move out of the cage. If the same particle has vacant space in its vicinity to which it can move, then it has a tendency to do so, leading to a relaxation-related movement. The free volume theory attempts to relate the vacant regions available to the diffusivity of the atoms; and hence to the relaxation of the system. Furthermore, it states that for an atom to participate in a relaxation motion, it has to at least move a distance that allows it to occupy a new region in space that only has a small overlap with the initial space. One of the assumptions used in the theory is that free volume can be redistributed without effecting free energy. There is no relation drawn between the local free energy of a particle and the free volume that is available to it.

CHAPTER III

EXPERIMENTAL DESIGN

Though there has been extensive research conducted to study the GFA and relaxation in BMGs, there has been no single study that analyzes the effect of alloying elements and their compositions on GFA. Attempts to study the relationship between relaxation and GFA with varying compositions and alloying elements still are required. Furthermore, there has been no significant effort to study structural changes in BMGs with relaxation (i.e. annealing), and how thermodynamic properties are affected by such relaxation processes.

3.1 Objectives and Methodology

The objective of this study is to determine the effect of composition and alloying element types on the glass forming ability (GFA) and the relaxation behavior of Zr-based metallic glasses. For this purpose metallic glasses consisting of Zr-Cu-Al and Zr-Ni-Al of varying composition have been made to determine the effect of Cu and Ni on GFA and relaxation behavior. Cu and Ni were chosen because they almost have the similar atomic radius of 128 pm and 124 pm, respectively. However, a large difference in the enthalpy of mixing with respect to the matrix element, Zr, exists when Cu replaces Ni. While the enthalpy of mixing of Cu in Zr is -78 KJ/mol, the enthalpy of mixing of Ni in Zr is -165 KJ/mol. As part of the study, samples of Zr-Pd-Al, Pd having an atomic radius of 137 pm and an enthalpy of mixing of -165 KJ/mol in Zr were also made. The specific research objectives are:

1. Characterization of the effects of Ni, Cu and Pd inclusion on the glass forming ability of Zr-based alloys.

2. Characterization of the annealing and composition effects on the relaxation behavior of Zr-based alloys.

3. Study the effects of annealing and composition on the structural features of Zr-based alloys using EXAFS.

4. Study the effect of alloying elements and annealing conditions on the electrical resistance of Zr-based alloys.

3.2 Sample Preparation

The BMG samples were prepared by using the melt spinning technique. The master alloy with the different compositions of Zr-Cu-Al, Zr-Ni-Al and Zr-Pd-Al were synthesized by arc melting the mixture in a purified argon atmosphere. The master alloy ingots were then melted and sprayed through a nozzle onto a copper wheel maintained at room temperature and rotating at 1800 rpm. The set up was operated in an argon atmosphere to prevent oxidation of the metal. The samples were obtained in the form of ribbons that had a width of 2 to 3 mm and thickness that varied between 30 - 80 μm.

Table 1 in the following page details the different alloying systems and their composition prepared for this study. The content of each alloying element is given in atomic percentages. E1 corresponds to Zr; E2 to Cu, Ni or Pd based on the system and E3 to Al.

Table 1 Composition of different alloying systems

Sample No	Alloy System	% E1	% E2	% E3
Sample 1	Zr-Cu-Al	70	16	14
Sample 2	Zr-Cu-Al	65	23	12
Sample 3	Zr-Cu-Al	60	30	10
Sample 4	Zr-Cu-Al	55	37	8
Sample 5	Zr-Cu-Al	50	46	4
Sample 6	Zr-Ni-Al	70	16	14
Sample 7	Zr-Ni-Al	65	23	12
Sample 8	Zr-Ni-Al	50	46	4
Sample 9	Zr-Pd-Al	70	16	14
Sample 10	Zr-Pd-Al	50	46	4

3.3 Experimental Set Up Description

This section describes the equipment used and the working principle behind the operation of each equipment. A differential scanning calorimeter (DSC), thermogravimetric analyzer (TGA), X-ray diffraction machine, extended X-ray absorption fine structure (EXAFS) and two-point electrical conductivity probe were used to measure GFA, thermal and structural relaxation and the resistivity of the samples.

3.3.1 Differential Scanning Calorimeter

Differential scanning calorimeter (DSC) is an instrument commonly used for thermal analysis of materials. It is used to measure temperatures of interest like the glass

transition temperature and melting temperature of mainly solids. It is also used to study phase transitions and measure properties like specific heat and enthalpy of a system.

As shown in Fig.5 the DSC consists of two pans, the specimen pan and the reference pan. Both of these pans are enclosed in an evacuated chamber with controlled heaters. The sample material is placed in the specimen pan, while the reference pan contains a material of known heat capacity and thermal behavior. There are thermocouples located beneath each pan to measure temperature at all times. The DSC maintains the same temperature rate for both pans while it measures the difference in heat flow required to maintain the temperature rate.

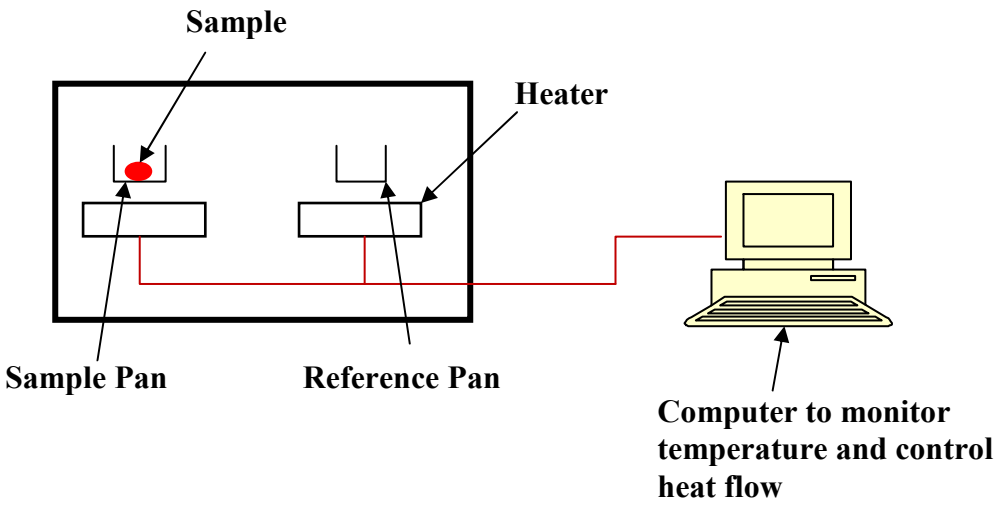

FIG.5 Schematic of differential scanning calorimeter

There are two kinds of transitions that can be observed when heating a material in a DSC, often called first and second order transitions. A first order transition is one in which there is release of latent heat as observed in during a crystallization process. A

first order transition is accompanied with a clear endothermic or exothermic peak. The second order transition involves only a change in the slope of the heat flow curve as it is routinely observed in glass transition processes. Fig.6 illustrates how glass transition, crystallization and melting would be displayed on a DSC thermograph.

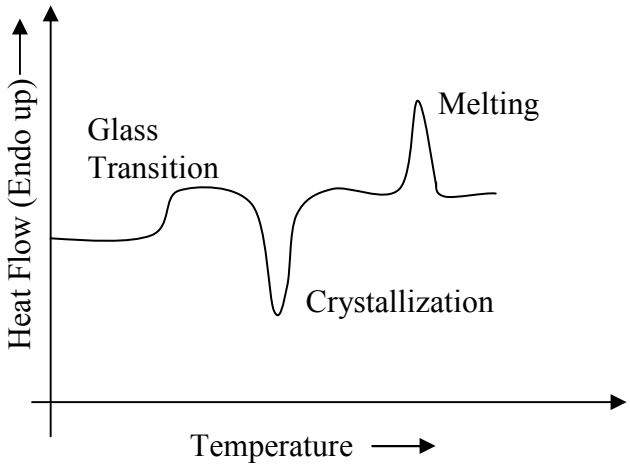

FIG.6 Features in a DSC curve

As shown in Fig.7, a Perkin Elmer Pyris 1 DSC that has an operating range from -60 to 600 °C was used to measure the glass transition temperature, crystallization temperature and heat capacity of all the samples. Copper pans that can be used in the temperature range of -180 to 725 °C were used as sample and reference pans. The Pyris I DSC is equipped with an intracooler that controls the flow of coolant through a circulating chamber and ensures reliable results.

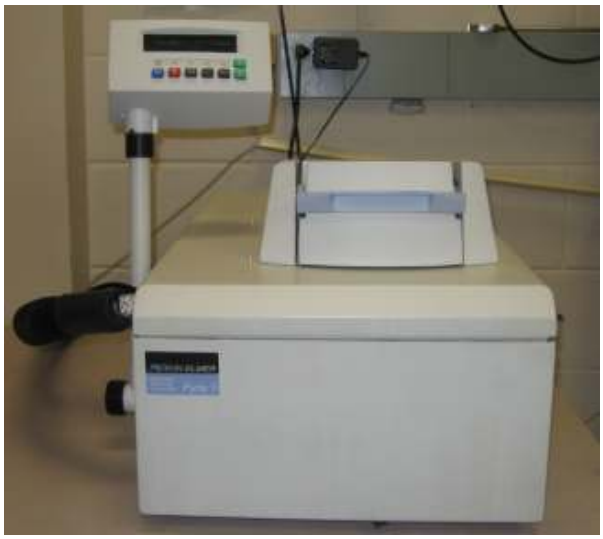

FIG.7 Pyris-1 Differential scanning calorimeter

FIG.8 Perkin Elmer AD 6 autosampler

The Perkin Elmer AD 6 autosampler shown in Fig.8 was used to measure the mass of the samples. It could provide measurements with an accuracy ± 0.001 mg. Specific heat measurements were conducted using DSC following ASTM-E-1269.

3.3.2 Thermogravimetric Analysis

A thermogravimetric analysis (TGA) measures mass changes in a material as a function of temperature or time under a controlled atmosphere. Like in a DSC, the analyzer here consists of 2 pans: sample and reference. The pans are placed on a high precision balance to monitor the mass and temperature of the samples. The pans are placed in an electrically heated oven. Each pan has a thermocouple mounted underneath to measure the temperature of the sample and the reference. In most experiments, inert gases like nitrogen or argon are purged to prevent oxidation or other undesired reactions. This overall set up is monitored and controlled by a computer system to achieve high accuracy measurements of different properties.

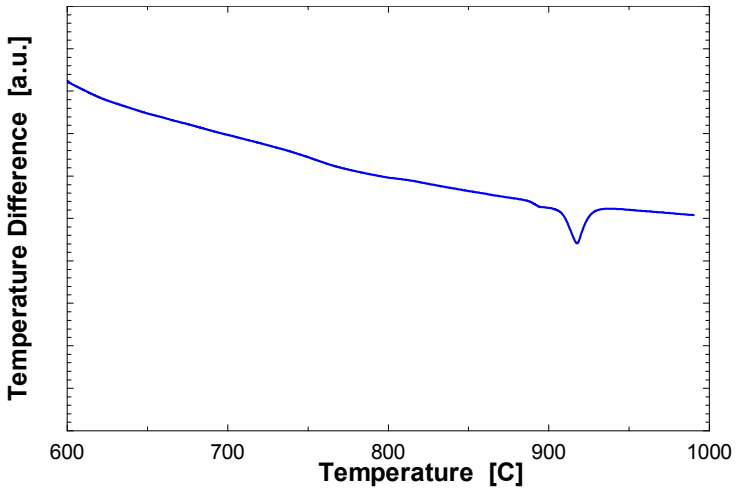

FIG.9 Melting process in a TGA graph

As shown in Fig.9 the melting process is a first order transition appears as an endothermic peak in a TGA graph.

FIG.10 TA TGA Q600

TA instruments TGA Q 600 shown in Fig.10 was used to measure the liquidus (T_L) temperature of the samples. The TGA has an operating range from ambient to 1500 °C. The balance has a sensitivity of 0.1 μg. It is equipped with a nitrogen gas purge system to avoid oxidation and other undesired reactions.

3.3.3 X-Ray Diffraction

The X-ray diffraction (XRD) is a non destructive analytical technique that is commonly used to study the arrangement of atoms in a crystal. Crystals have a regular periodic arrangement of atoms. X-rays have a wavelength of a few angstroms, which is comparable with the atomic distances in a crystal. As shown in Fig.11, when an X-ray beam is focused on to a sample the incident X-rays interact with the atoms and get

diffracted. The diffraction or scattering occurs primarily through the electrons in the atoms.

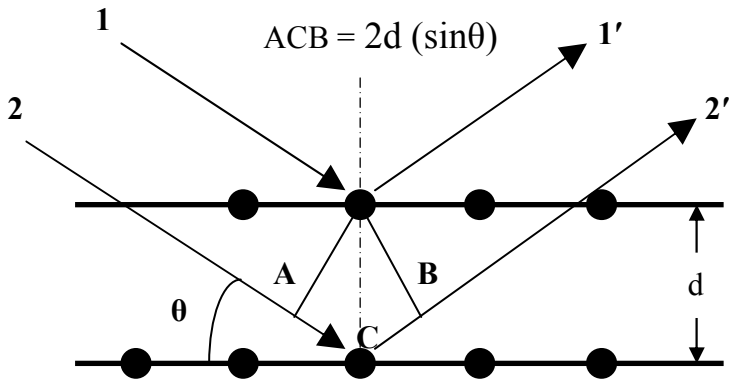

FIG.11 Schematic of parallel rays reflected across atomic planes

The X-rays that are diffracted from the atoms interfere to give a diffracted beam. This was first discovered by W.L.Bragg in 1912 who deduced a law for X-ray diffraction, which is called Bragg's Law. The law states that $n\lambda = 2d \sin\theta$ where, d is the distance between atomic planes (in Å), λ is the wavelength of the incident X-rays (in Å), θ is the angle of diffraction (in deg.) and n is an integer.

Diffractometer is used to study the structure of a crystal from the diffraction spectrum obtained from an X-ray beam interacting with the crystal atoms. It mainly consists of a source of radiation, a monochromator to adjust the wavelength, slits to adjust the beam shape, sample holder and a detector/counter. The source emits the X-rays on to the crystal, which are diffracted by the atomic planes in the crystal.

The detector detects the diffracted beam and then records it with respect to the angle at which it is positioned from the source (2θ). The intensity of the diffracted beam is plotted with respect to the position (2θ) of the rotating diffractometer and the graph obtained can be analyzed to obtain the crystal structure.

FIG.12 Bruker D8 diffractometer

As shown in Fig.12, a Bruker D8 diffractometer with a CuKa radiation was used for the purpose of detecting whether the samples were amorphous. A LynxEYE detector was used for the data collection. A zero-background sample holder was used for mounting the sample.

Figs.13 and 14 in the following page illustrates the XRD graph obtained from a Bruker D8 diffractometer. The graph shows a broad halo in the case of an amorphous

sample. The presence of any crystalline content in the sample shows up as sharp peaks in the XRD graph.

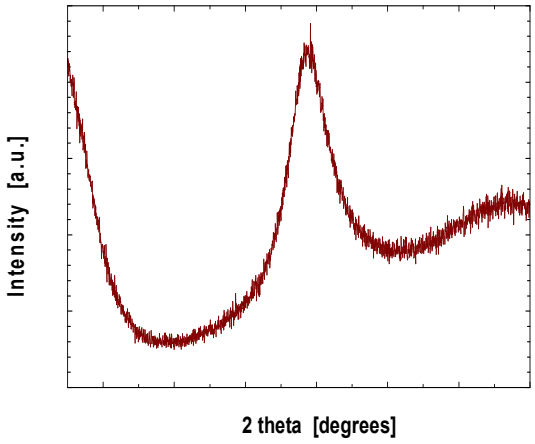

FIG.13 XRD graph of amorphous sample

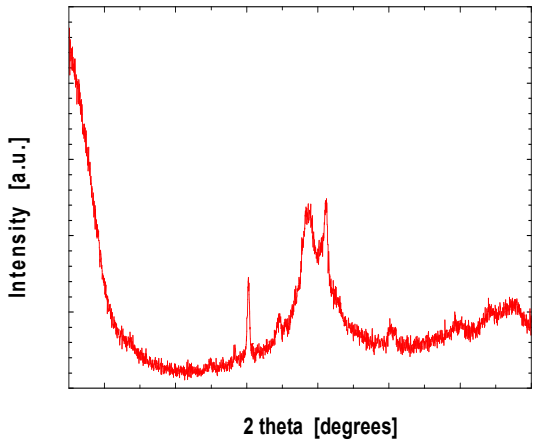

FIG.14 XRD graph of crystalline sample

3.3.4 Extended X-ray Absorption Fine Structure

XAFS spectroscopy is normally used to measure the fine structure associated with one of the characteristic X-ray absorption edges of an element of interest. The

parameters that are found by this method include atomic number, interatomic distance and coordination number of the atoms surrounding the particular element being probed. The fine structure is usually of two types. There is a fine structure which is associated with the absorption edge which is called as X-ray absorption near-edge structure (XANES). The second fine structure consists of a weak periodic oscillatory structure that occurs above the main edge and decreases in intensity the further it is away from the main edge, which is called as the extended X-ray absorption fine structure (EXAFS). Either or both of these regions of the XAFS spectrum can be used to determine the structural configuration of the element in a material. The analysis of each region (EXAFS and XANES) is an independent study by itself. Typically, the XAFS spectrum is normalized and then divided into separate XANES and EXAFS regions. Fig.15 illustrates the division of Selenium (Se) spectrum into XANES and EXAFS regions. The portion of the spectrum contained in the dotted box is used for XANES analysis while the spectrum at the higher energy range is used for EXAFS analysis. The EXAFS region can be further analyzed mathematically by obtaining a radial structure function (RSF) using Fourier transformation within the EXAFS region. Fig.16 shows the RSF spectrum for Se. The peak in the RSF spectrum is considered to be a one-dimensional representation of the local environment around the Se atom. While the EXAFS region provides structural information, the XANES region provides bonding and valence information.

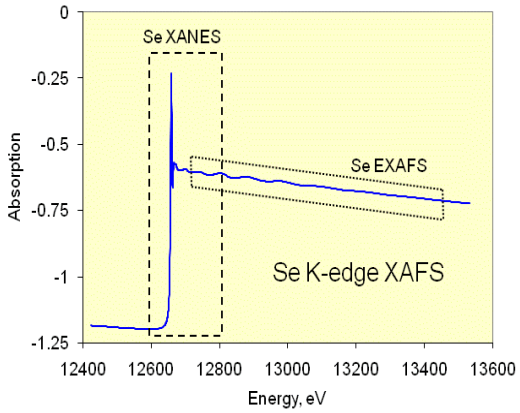

FIG.15 XAFS spectrum of elemental Se

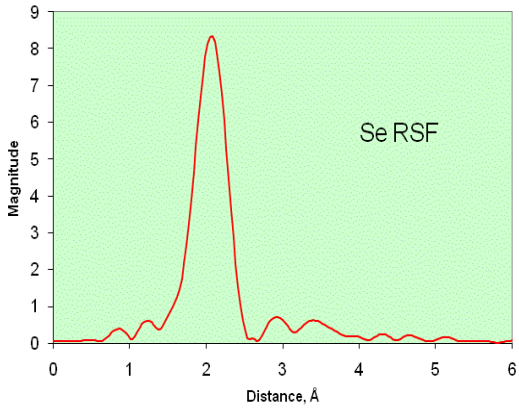

FIG.16 RSF spectrum of elemental Se

For this study, Zirconium XAFS measurements were made using the beam-line X-18B of the National Synchrotron Light Source (NSLS) at Brookhaven National Laboratory, NY. A schematic representation of the set up is shown in Fig.17.

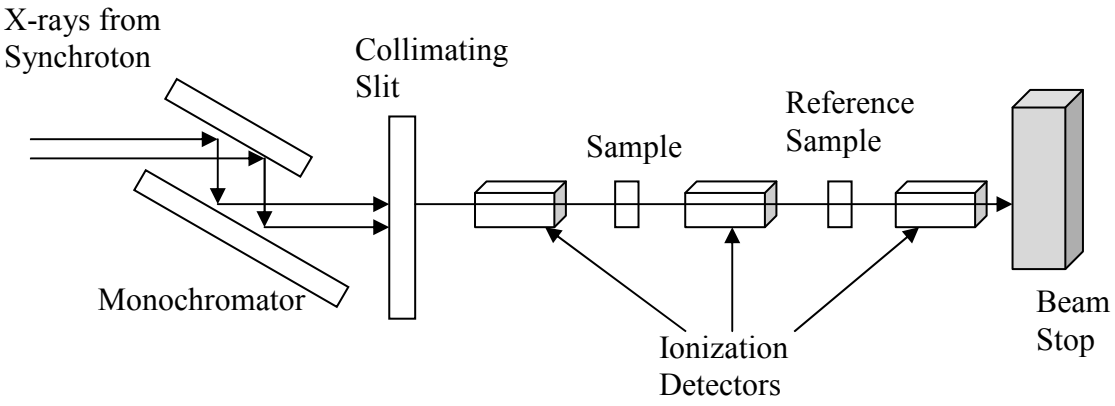

FIG.17 Schematic representation of XAFS set up

Gas ionization detectors were used to measure the X-ray intensity before (I_0) the sample and after (I_t) transmission through the sample. The spectra were recorded over the energy range from 200 eV below the Zr K-edge edge at 17,998 eV to 850 eV (15 k) above the edge using the rotation of the Si(111) double crystal monochromator to vary the energy. A foil of zirconium metal was used to calibrate the energy scale of the spectrum. The absorption spectrum of the Zr metal foil was subtracted from the test sample spectrum to normalize the spectrums. The spectrum was then divided into the XANES and EXAFS region. The Fourier transformation was used to obtain a radial structure function (RSF). The RSF can be used to study the effect of annealing on the structure of BMGs. The processing was done using the program Sixpack, a program normally used for XAFS analysis.

3.3.5 Two Point Probe

The electrical resistance of the BMGs was measured to understand the effects of relaxation and alloying element inclusion on it. The two point probe was used to measure the sheet resistance of the metal strips.

As shown in Fig.18, it consists of two probes of finite radius. The probes are spring loaded to minimize sample damage and apply constant force during measurements. A high impedance current source is used to apply a constant voltage (V) across a metal strip and the flow of current (I) through the strip is measured. The resistance of the strip can then be calculated by using the relation V= I*R, where R correspond to the resistance of the strip.

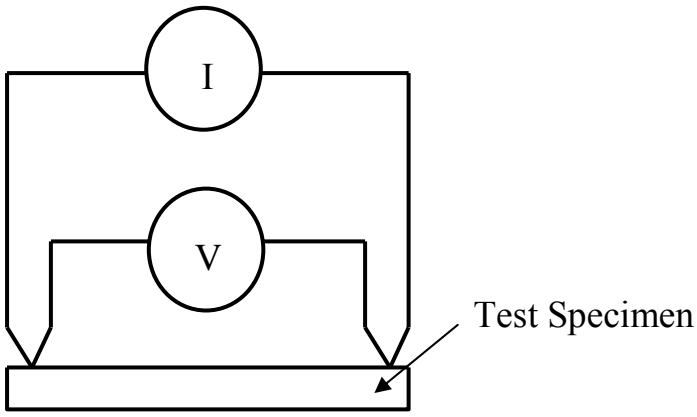

FIG.18 Two point probe for resistance measurement

The two point probe used for the current study consisted of two probes made of tungsten carbide separated by a distance of 1.02 mm (0.040 inches). The probe tip radius was 0.04 mm (0.0016 inches). The voltage and current was controlled by a data acquisition system to measure the resistance of the strip. The probe is mounted on a spindle that has a graduated thimble to precisely control the vertical movement of the probe.

3.4 Experimental Approach

All the samples obtained from melt spinning were in the form of ribbons. The amorphous nature of each sample was verified to be amorphous by X-ray diffraction (XRD) technique. A small strip of the ribbon was mounted on the specimen holder of the XRD machine. The sample was probed for a 2θ angle of 70°. After verifying the lack of long-range order of all the amorphous metallic alloys, other important tests were conducted to understand the effects of relaxation on all the samples.

3.4.1 Assessment of Glass Forming Ability (GFA)

Thermal analysis techniques were used to obtain data to be able to compare the glass forming ability of the samples as prepared. Differential scanning calorimeter (DSC) was used to measure T_g (glass transition temperature) and T_x (crystallization temperature) of the samples as prepared. Copper pans that have an operating range of -180 °C to 725 °C were used for the tests. The DSC was purged with nitrogen gas at 20 ml/min to avoid oxidation or other undesired results. Heat and temperature flow calibration runs were performed using indium. A baseline run was undertaken using empty pans placed in the sample and reference cells within the temperature range of interest. Each sample of Zr-Cu-Al and Zr-Ni-Al was scanned from 300 °C to 550 °C at the rate of 20 °C/min to obtain T_g and T_x. A sample mass between 12 and 15 mg was used. The samples after conducting DSC experiments were subject to XRD tests to make sure each sample crystallized after exceeding the crystallization temperature.

The liquidus temperature (T_l) of the samples was found using thermogravimetric analysis (TGA) as mentioned earlier. The TGA was purged with nitrogen at 100 ml/min

to avoid oxidation of the samples. The sample size was nominally 10 mg and the heating rate was 20 °C/min. TGA experiments were carried out until each sample completely melted. The melting shows as an endothermic peak on the TGA thermograph for each sample as shown in Fig.9. TGA and DSC results were used to obtain the values for the GFA parameters T_{rg} (reduced glass transition temperature) and γ. Furthermore, these values were compared to determine which alloy system and composition yielded higher relative GFA.

3.4.2 Thermal Relaxation Studies

The main objective of the study was to understand the effects of alloying elements, annealing temperature and annealing time on the thermal relaxation of BMGs. Previous studies have shown that the enthalpy recovery increases with annealing time and temperature; however little information is available in regards to the effect of alloying element type on thermal relaxation. For this purpose, samples of $Zr_{65}Cu_{23}Al_{12}$ and $Zr_{65}Ni_{23}Al_{12}$ were used for the study. The samples were verified to be amorphous by XRD technique. Each sample was then sealed with Argon in a quartz tube and heated to 690 K (approximately 30 K above the T_g) in a well controlled furnace at 10 °C/min and cooled immediately to room temperature to ensure uniform thermal history for all the samples. The samples were then again sealed with Argon in quartz tubes and annealed at 600 K (approximately 60K below T_g) for 0.5 hr, 2 hr, 4 hr, 10 hr and 18 hr in a well controlled furnace. The amorphous nature of the samples was confirmed by XRD technique after annealing. Also, a crystalline batch of samples was obtained by heating the samples at 1073 K (above crystallization temperature) for 30 minutes. The purpose

of the crystalline batch was to compare the variation in heat capacity and enthalpy between the as-obtained amorphous sample and the crystallized sample. Also, the crystallized samples were used to study how they differ in structure from the amorphous samples using EXAFS studies.

The specific heat values of the as-obtained sample and the annealed samples were found using DSC. The sample mass used for each test was between 12 and 15 mg. The intracooler was turned on to maintain steady state conditions during the experiment. The DSC was preconditioned by running heat-cool cycles in the area of interest for around 45 minutes. The specific heat values were measured over the temperature range of 300 °C to 450 °C at a heating rate of 10 °C / min. ASTM E 1269 method was used to find the specific heat of the samples. The method involved running three consecutive runs, which were: a baseline with empty pans, followed by running a sapphire standard, and then running the sample specimen. The mass of sapphire was nominally 6 mg, while the test specimen mass was in the range of 12 to 15 mg. The Pyris specific heat software was used to calculate the specific heat from the collected data.

Also the activation energy for relaxation was found by using the Kissinger analysis. Sample 2 and 7 annealed at 600 K for 18 hr were heated at different heating rates in the DSC. The heating rates used were 10, 30, 50 and 75 °C / min. The shift in the glass transition peak of the DSC was measured and then using the Kissinger equation the activation energy for relaxation was found.

3.4.3 EXAFS Studies

The purpose of this study was to assess the effects of alloying elements, annealing temperature and annealing time on the structure of BMGs. Past research has shown different phenomena in BMGs including changes in the short range order of atoms, to changes in the free volume of BMGs after annealing. However, studies to date have provided insufficient information to conclusively establish which of the two main phenomena is responsible for the structural changes that occur in BMG after annealing. In an effort to elucidate the true nature of the annealing behavior of BMGs, EXAFS analysis was undertaken to provide more information on structural relaxation in these BMG samples. For this study, samples of $Zr_{65}Cu_{23}Al_{12}$ and $Zr_{65}Ni_{23}Al_{12}$ were tested using EXAFS. The as-obtained, the samples annealed at 600 K for 2h and 18h were probed by the extended X-ray absorption fine structure (EXAFS) technique. The Zr-edge in each sample was probed to observe changes in the local environment around Zr in these structures. The Zr-edge of the crystal structures of these samples were also probed for the purpose of better understanding the structural changes in the relaxed amorphous samples. Annealed BMG ribbon's approximately 70 μm thick, and with a length greater than 15 mm were carefully positioned in the sample holder to ensure good interaction between the beam and the strip. Low intensity X-rays were used and transmitted because the sample thicknesses were slightly higher than that those routinely used for EXAFS studies. In order to compensate for the thickness difference, the spectrum was recorded in triplicates and averaged to obtain more precise readings. The X-ray beam dimensions were set to 10 mm x 0.5 mm by using the beam-line slit assembly. The spectra were

recorded over the energy range from 200 eV below the Zr K-edge to 850 eV above the edge by rotating the Si double crystal monochromator.

3.4.4 Resistance Measurements

Resistance measurements were conducted to understand the effect of composition and annealing conditions on the electrical properties of BMGs. The two point probe was used for resistance measurements. Each sample was cleaned and placed below the probe. The probe was then lowered using the thimble. The probe was pushed to the same depth by rotating the thimble to the same point on the scale every time. A constant voltage of 0.175 V was applied across the probe for each sample and the data acquisition system would then sense the current from which the resistance was measured. Three resistance measurement trials were conducted for each sample. The resistance values of samples 1 through 8 were measured to compare how resistance varies with changes in composition and alloying element. Also, the resistance of samples 2 and 7 annealed at 600K for 2 hr and 18 hr were measured to understand how resistance changes with relaxation. The resistance of the crystalline structures of samples 2 and 7 were also measured to compare the variation of resistance between the amorphous and crystalline structures.

CHAPTER IV

RESULTS AND DISCUSSION

This chapter presents all the data collected for studying GFA and relaxation of BMGs, and discusses the results in the context of past research and fundamental theories.

4.1. XRD Graph of Samples

All the BMG samples obtained from melt spinning were tested using XRD technique to verify that they were amorphous. A Bruker D8 diffractometer was used for this study. The XRD graph for an amorphous sample should show no sharp diffraction peaks as established by other researchers in the field [31, 32]. The presence of any sharp peaks is an indication of crystalline phases in a sample. The XRD graphs for the Zr-Cu-Al samples of different composition are shown in Figs. 19 to 23.

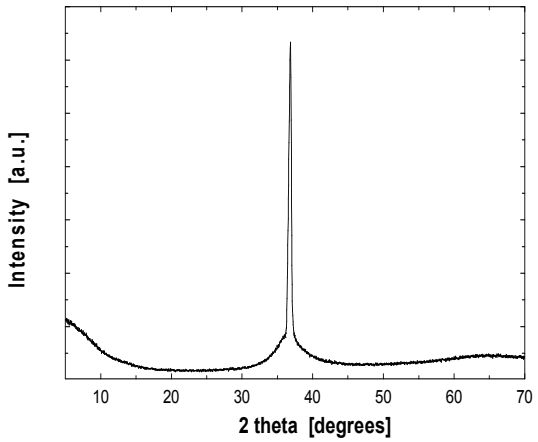

FIG.19 XRD graph of as-is $Zr_{70}Cu_{16}Al_{14}$ (Sample1)

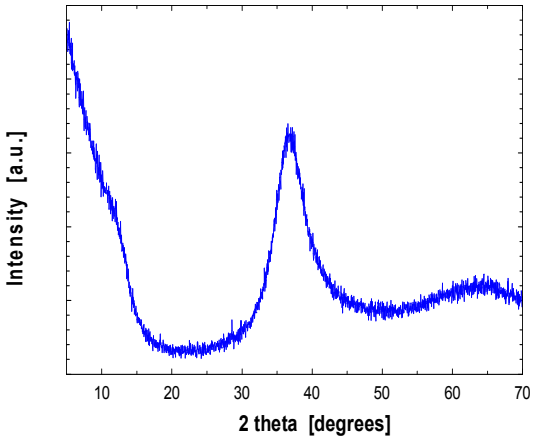

FIG.20 XRD graph of as-is $Zr_{65}Cu_{23}Al_{12}$ (Sample 2)

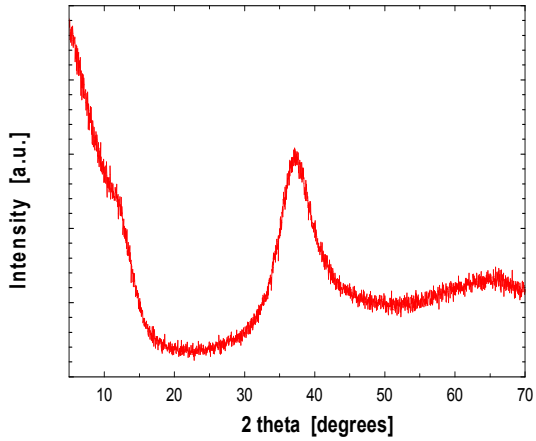

FIG.21 XRD graph of as-is $Zr_{60}Cu_{30}Al_{10}$ (Sample 3)

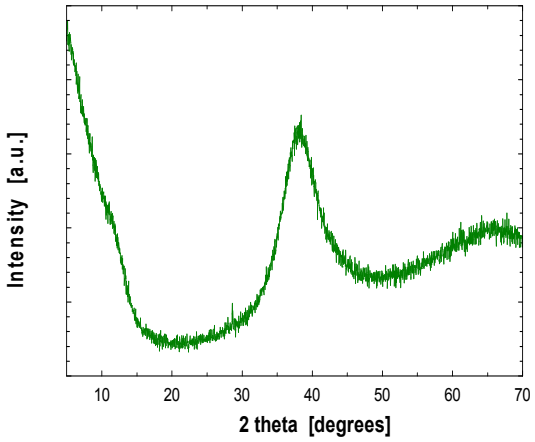

FIG.22 XRD graph of as-is $Zr_{55}Cu_{37}Al_8$ (Sample 4)

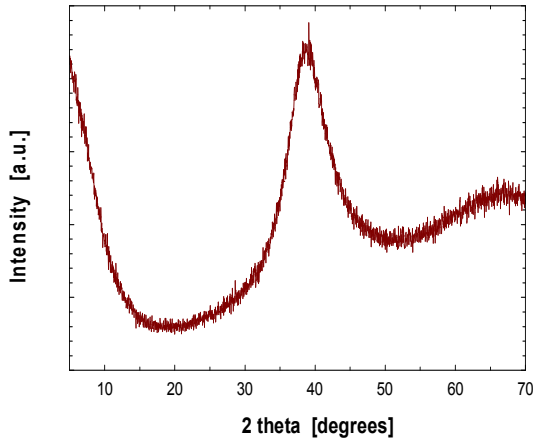

FIG.23 XRD graph of as-is $Zr_{50}Cu_{46}Al_4$ (Sample 5)

As seen in Fig.19, the sample $Zr_{70}Cu_{16}Al_{14}$ shows a broad halo and a single sharp peak, which is an indication of some degree of crystallinity existing within the amorphous sample. The XRD graphs of the remaining samples are shown in Figs.20 to 23 which exhibit a broad halo, indicative of a stable amorphous phase in these samples.

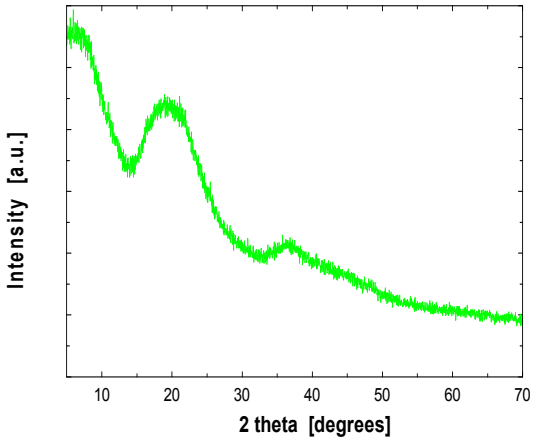

FIG.24 XRD graph of as-is $Zr_{70}Ni_{16}Al_{14}$ (Sample 6)

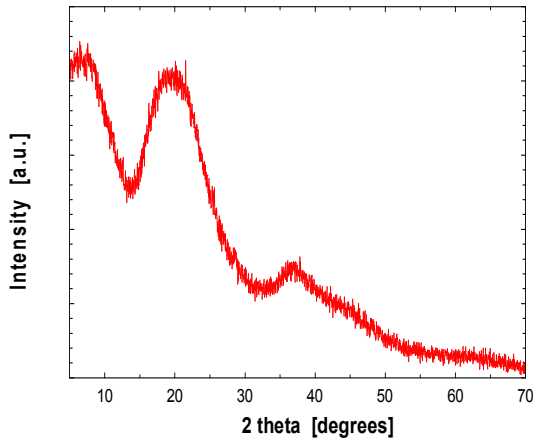

FIG.25 XRD graph of as-is $Zr_{65}Ni_{23}Al_{12}$ (Sample 7)

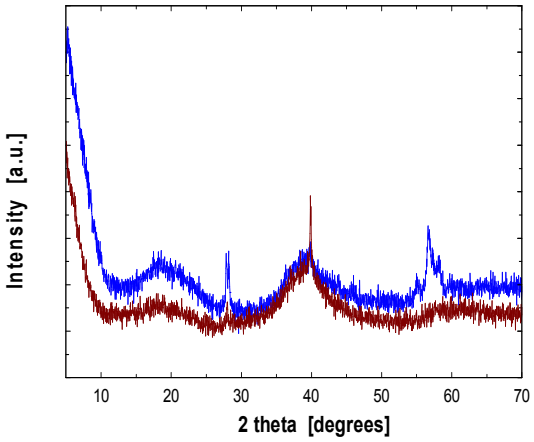

FIG.26 XRD graph of as-is $Zr_{50}Ni_{46}Al_4$ (Sample 8)

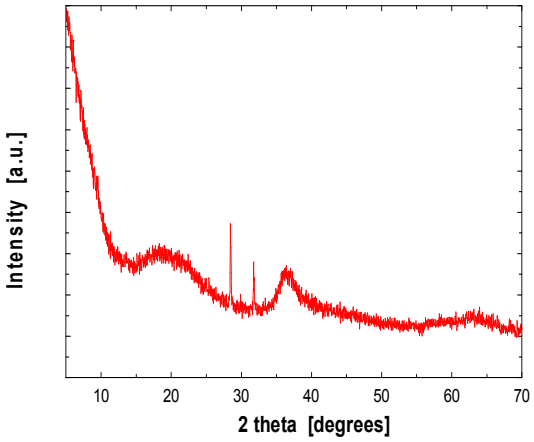

FIG.27 XRD graph of as-is $Zr_{70}Pd_{16}Al_{14}$ (Sample 9)

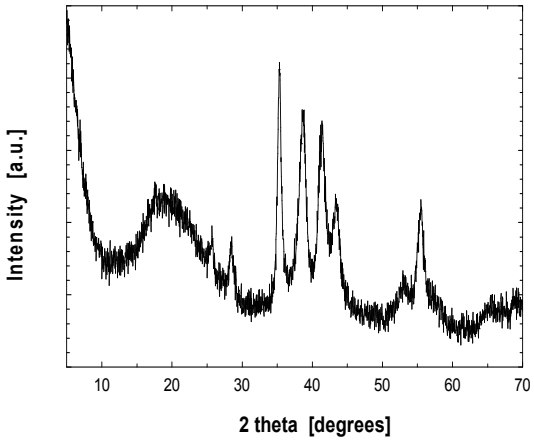

FIG.28 XRD graph of as-is $Zr_{50}Pd_{46}Al_4$ (Sample 10)

The XRD graphs of the Zr-Ni-Al and Zr-Pd-Al samples are shown in Figs. 24 to 28. The BMG samples $Zr_{70}Ni_{16}Al_{14}$ and $Zr_{65}Ni_{23}Al_{12}$ appear to be amorphous. The XRD graph of sample $Zr_{50}Ni_{46}Al_4$ in Fig.25 shows sharp peaks indicating some degree of crystallinity. More importantly, the XRD graph of this sample for two different trials showed variations in peak position. This could be due to insufficient mixing of the melt, leading to a non uniform sample. The XRD graphs of the Zr-Pd-Al samples show existence of multiple sharp peaks, indicating poor glass forming ability of these alloys. As a result of the apparent high degree of crystallinity in these structures, there was no clear T_g or T_l observed for these samples in the DSC and TGA graphs, respectively. As a result these samples were not used for comparative studies of GFA and relaxation.

4.2 Glass Forming Ability (GFA) Study

To compare the GFA of the BMG samples consisting of different alloying elements and composition, the GFA indicator γ and T_{rg} were calculated. For this purpose

the T_g, $T_{x,}$ and T_l of the samples were measured using DSC and TGA . The DSC was used to find the T_g and T_x of the BMG as-is samples. The samples were heated at 20 °C/min in the DSC in the temperature range of interest. The graphs obtained from the experiment are shown below:

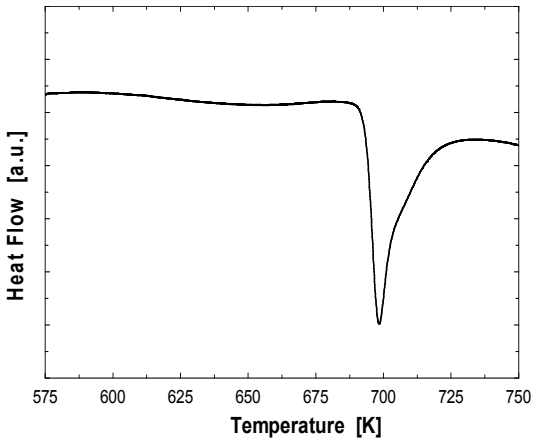

FIG.29 DSC graph of as-is $Zr_{70}Cu_{16}Al_{14}$ (Sample 1)

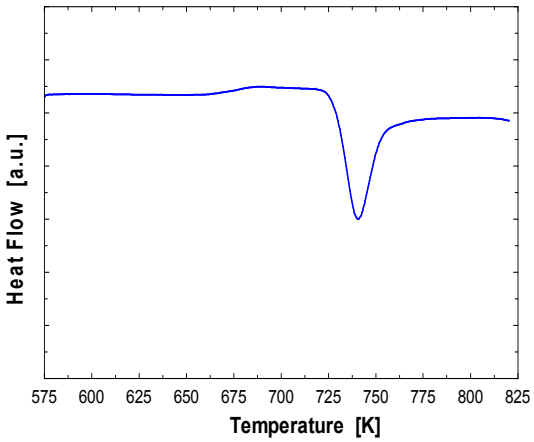

FIG.30 DSC graph of as-is $Zr_{65}Cu_{23}Al_{12}$ (Sample 2)

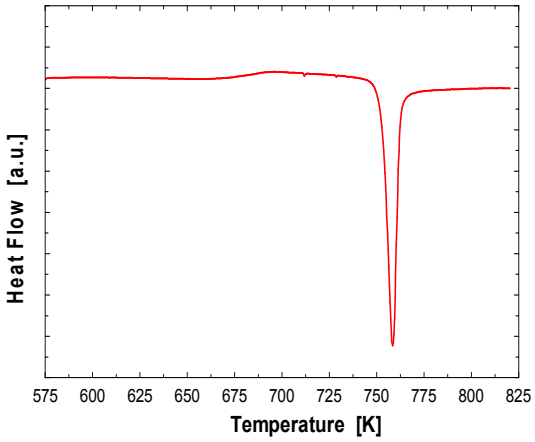

FIG.31 DSC graph of as-is $Zr_{60}Cu_{30}Al_{10}$ (Sample 3)

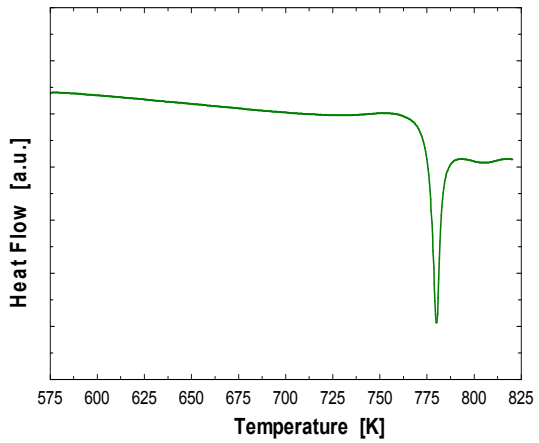

FIG.32 XRD graph of $Zr_{55}Cu_{37}Al_8$ (Sample 4)

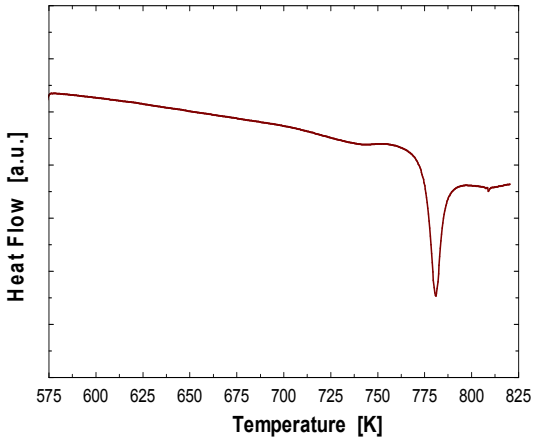

FIG.33 DSC graph of as-is $Zr_{50}Cu_{46}Al_4$ (Sample 5)

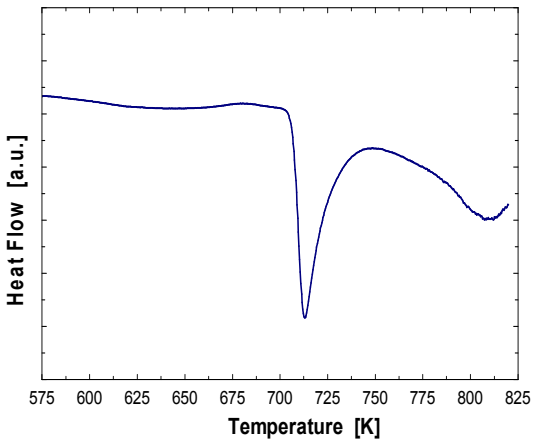

FIG.34 DSC graph of as-is $Zr_{70}Ni_{16}Al_{14}$ (Sample 6)

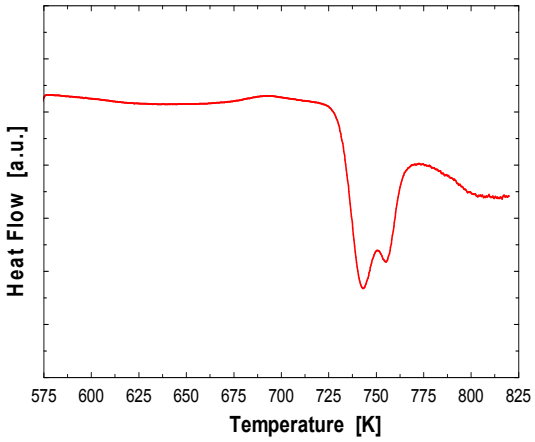

FIG.35 DSC graph of as-is $Zr_{65}Ni_{23}Al_{12}$ (Sample 7)

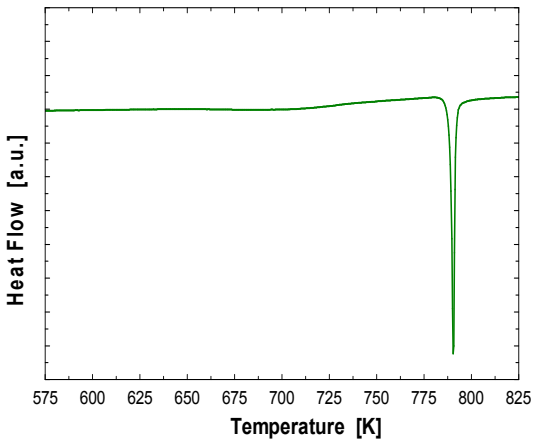

FIG.36 DSC graph of as-is $Zr_{50}Ni_{46}Al_4$ (Sample 8)

The DSC thermographs for varying compositions of Zr-Cu-Al and Zr-Ni-Al are shown in Figs.29 through 36. The DSC graphs confirm the glassy nature of the BMG

samples since a slight monotonic change in the slope of the heat flow curve can be observed in all the samples. The change in slope is used to identify the characteristic glass transition point (endothermic event). Glass transition is followed by crystallization (exothermic event), which is also evident in DSC thermographs. The glass transition and crystallization temperature points were measured from the DSC graph. From Figs.29 to 36, it can be observed that the crystallization peaks become shaper with a decrease in Zr content. This is indicative of an increase in the kinetics of crystallization [33] and a reduction in the corresponding crystallization energy barrier.

To confirm the samples had crystallized after the DSC tests, XRD was performed on the samples again. As seen in Figs.37 to 44 sharp peaks were observed on the XRD graph confirming the samples had crystallized.

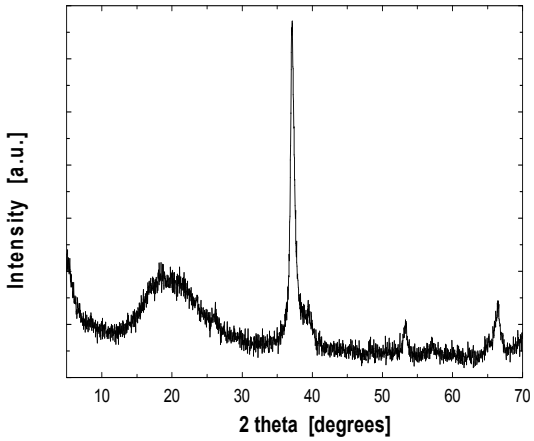

FIG.37 XRD graph of crystallized $Zr_{70}Cu_{16}Al_{14}$ (Sample 1)

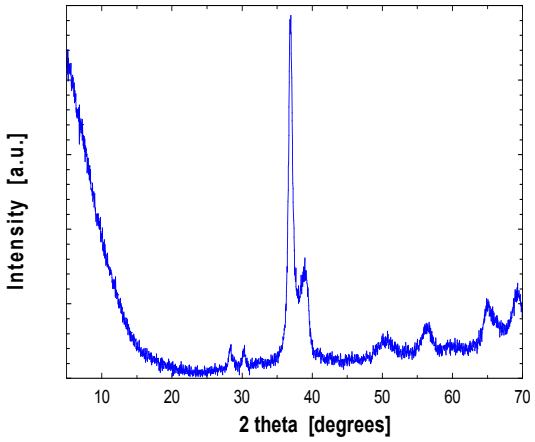

FIG.38 XRD graph of crystallized $Zr_{65}Cu_{23}Al_{12}$ (Sample 2)

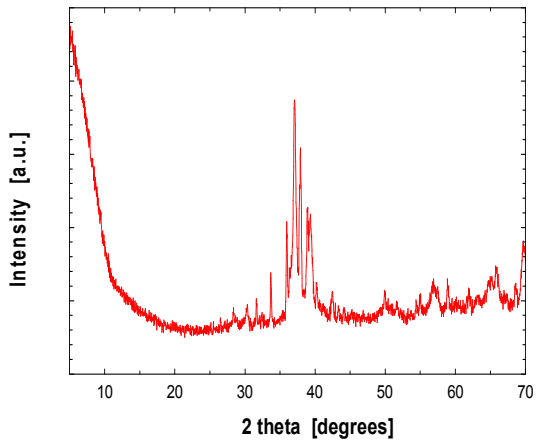

FIG.39 XRD graph of crystallized $Zr_{60}Cu_{30}Al_{10}$ (Sample 3)

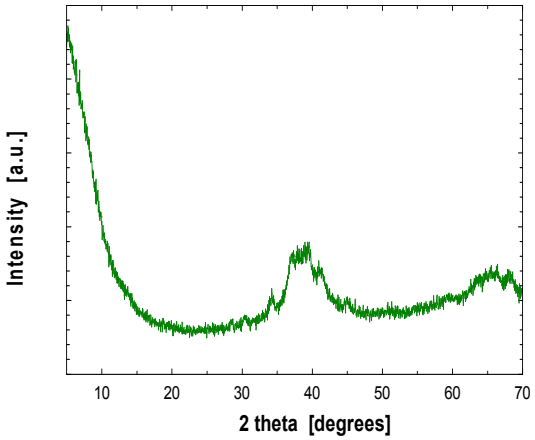

FIG.40 XRD graph of crystallized $Zr_{55}Cu_{37}Al_8$ (Sample 4)

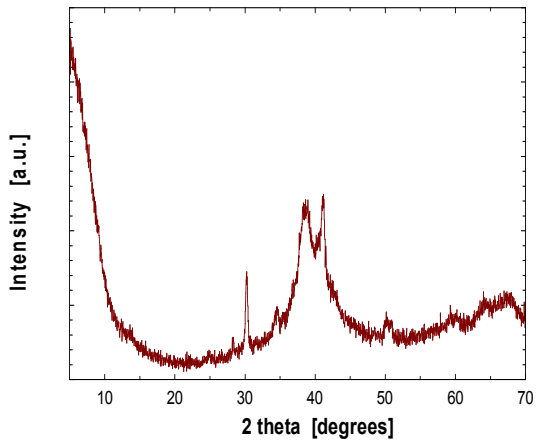

FIG.41 XRD graph of crystallized $Zr_{50}Cu_{46}Al_4$ (Sample 5)

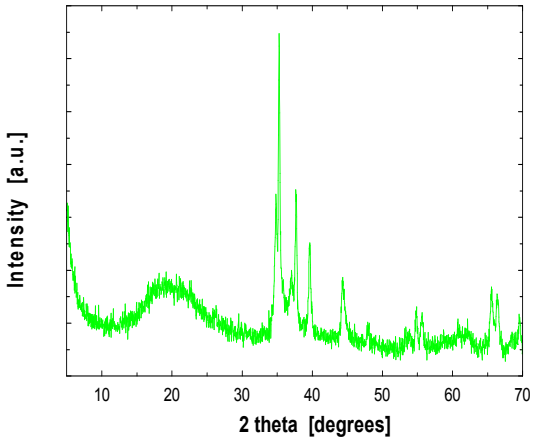

FIG.42 XRD graph of crystallized $Zr_{70}Ni_{16}Al_{14}$ (Sample 6)

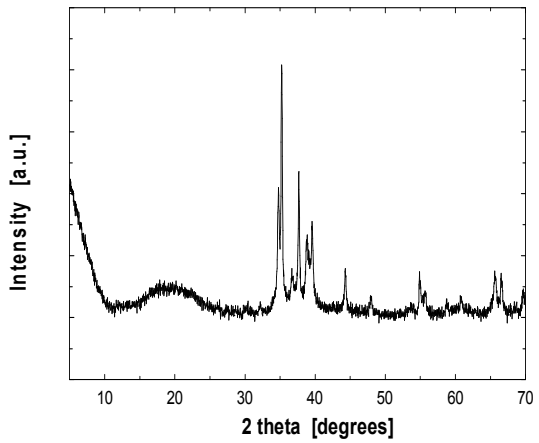

FIG.43 XRD graph of crystallized $Zr_{65}Ni_{23}Al_{12}$ (Sample 7)

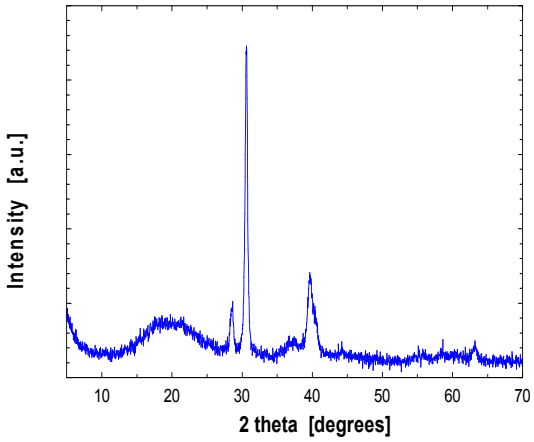

FIG.44 XRD graph of crystallized $Zr_{50}Ni_{46}Al_4$ (Sample 8)

To calculate the GFA parameters, it is also essential to know the T_l (liquidus temperature) of the samples. For this purpose the as-obtained BMG samples were heated at a rate of 20 °C/min in a TGA until melting was evident on the TGA graph. The TGA graphs obtained are shown below:

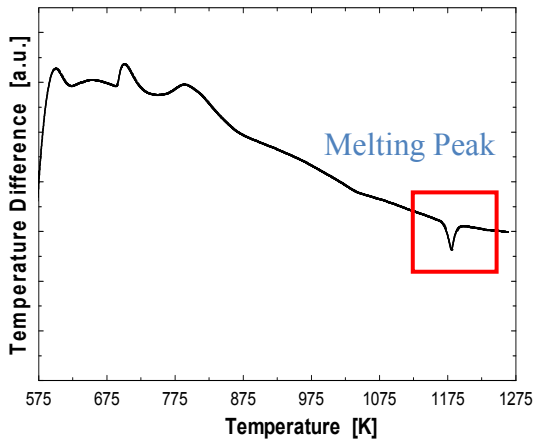

FIG.45 TGA graph of as-is $Zr_{70}Cu_{16}Al_{14}$ (Sample 1)

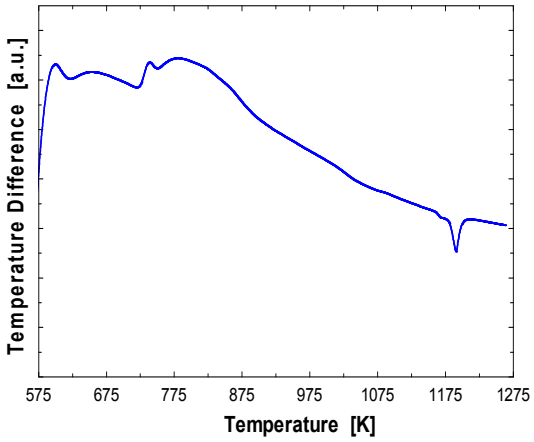

FIG.46 TGA graph of as-is $Zr_{65}Cu_{23}Al_{12}$ (Sample 2)

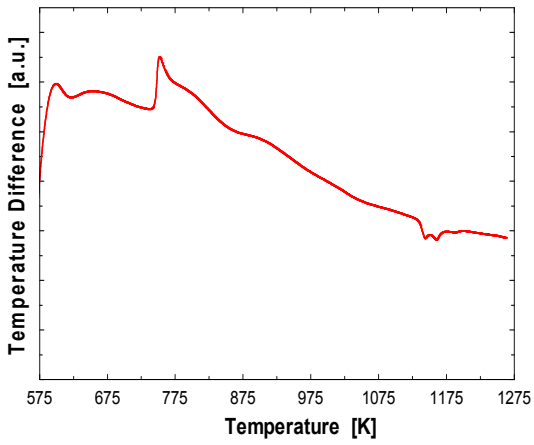

FIG.47 TGA graph of as-is $Zr_{60}Cu_{30}Al_{10}$ (Sample 3)

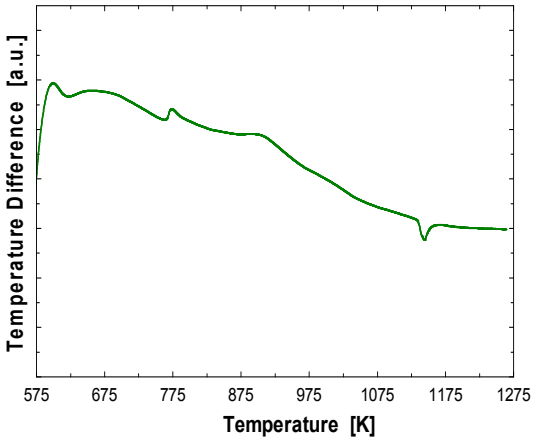

FIG.48 TGA graph of as-is $Zr_{55}Cu_{37}Al_8$ (Sample 4)

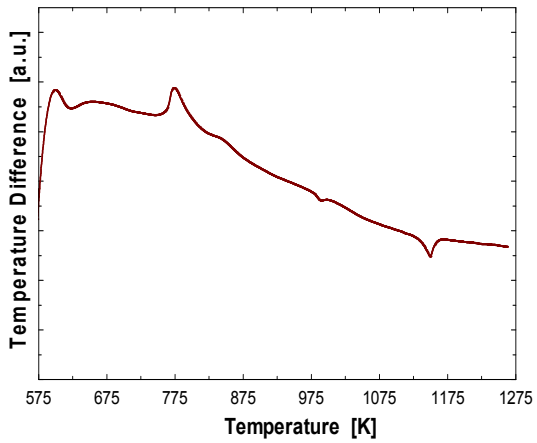

FIG.49 TGA graph of as-is $Zr_{50}Cu_{46}Al_4$ (Sample 5)

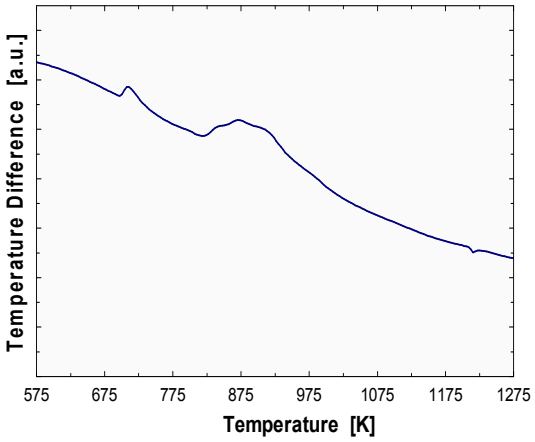

FIG.50 TGA graph of as-is $Zr_{70}Ni_{16}Al_{14}$ (Sample 6)

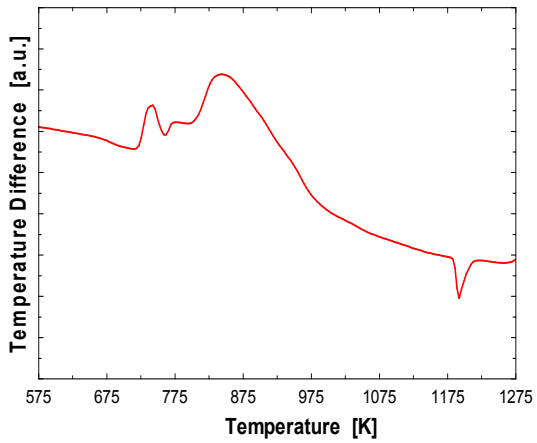

FIG.51 TGA graph of as-is $Zr_{65}Ni_{23}Al_{12}$ (Sample 7)

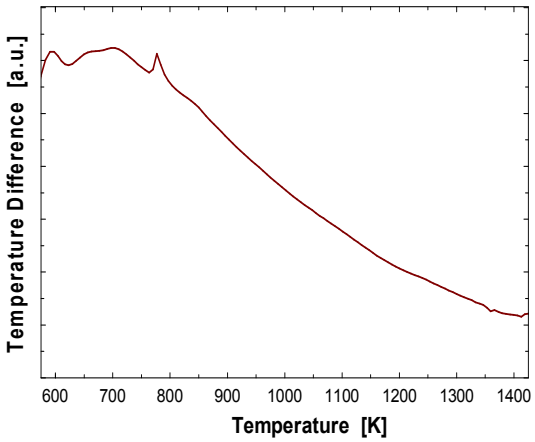

FIG.52 TGA graph of as-is $Zr_{50}Ni_{46}Al_4$ (Sample 8)

In the TGA graphs shown in Figs.45 to 52 the melting process is evident as an endothermic event. The liquidus temperature point (T_l), which is the offset temperature of the melting process (when the melting is complete) was measured from the TGA graph [33].

The T_g, T_x and T_l of the Zr-Cu-Al and Zr-Ni-Al BMG samples measured using the DSC and TGA are summarized in Table 2. Also, Table 2 presents the GFA indicators calculated from T_g, T_x, and T_l temperature points. The GFA indicators a) supercooled liquid region ΔT_x defined as $\Delta T_x = T_x - T_g$, b) the reduced glass transition temperature T_{rg} defined as $T_{rg} = \frac{T_g}{T_l}$ and c) γ defined as $\gamma = \frac{T_x}{T_g + T_l}$ are provided in the table.

Table 2 Summary of characteristic temperatures and GFA indicators for the as-is BMG samples

Sample No	Alloy System	T_g (K)	T_x (K)	T_l (K)	ΔT_x (K)	T_{rg}	γ
1	$Zr_{70}Cu_{16}Al_{14}$	656	690	1192	34	0.550	0.373
2	$Zr_{65}Cu_{23}Al_{12}$	660	724	1203	64	0.548	0.389
3	$Zr_{60}Cu_{30}Al_{10}$	669	741	1169	72	0.572	0.403
4	$Zr_{55}Cu_{37}Al_{8}$	731	759	1155	28	0.633	0.402
5	$Zr_{50}Cu_{46}Al_{4}$	740	771	1159	31	0.638	0.406
6	$Zr_{70}Ni_{16}Al_{14}$	659	706	1216	48	0.542	0.377
7	$Zr_{65}Ni_{23}Al_{12}$	666	729	1204	64	0.553	0.390
8	$Zr_{50}Ni_{46}Al_{4}$	707	785	1359	77	0.520	0.380

As seen in Table 2, BMG samples 2, 3, 6, 7 and 8 have a large supercooled liquid region $\Delta T_{x,}$ that exceeds 45 K which is a good indication of their thermal stability against crystallization[34]. The large supercooled liquid region in BMGs is attributed to the formation of a liquid with a high dense random packing, which is uniformly distributed over the long range but it has a significantly different atomic configuration than the crystalline counterparts [35]. While the Zr-Cu-Al does not show any trend for ΔT_x, the ΔT_x tends to increase with a decrease in Zr content (or increase in Ni content) for the Zr-Ni-Al samples. Also, it is seen that Zr-Ni-Al alloy compositions have a higher supercooled liquid region than the Zr-Cu-Al alloy compositions of same composition. However, in general it has been found that ΔT_x is indicative of the thermal stability against crystallization but as claimed by Waniuk et al. [10] is not an accurate indicator of

GFA for BMGs . The reduced glass transition temperature T_{rg} is close to 0.6 for all the samples, which has been found to be the case for most metallic glasses [2]. The T_{rg} values for the Zr-Cu-Al systems and Zr-Ni-Al system are quite similar for different compositions.

As mentioned in the literature review, the GFA indicator γ has been found to be the most reliable for a variety of alloying systems. The higher the value of γ, the higher the GFA of the system is considered to be. From past research, it has been found that the value of γ is in the range between 0.350 and 0.500 for a variety of BMG alloy systems [10]. From Table 2, the γ value for all the BMG seem to fall in the same range of 0.35 to 0.50. The γ value seems to have an increasing trend with decreasing Zr content in the Zr-Cu-Al alloy system (samples 1 – 5) while no exact trend can be observed for γ in the Zr-Ni-Al system (samples 6 – 8) . Based on the values of γ, it appears that sample 5 has the best GFA while sample 1 has the lowest GFA in the Zr-Cu-Al alloy system. When correlated with the XRD results, it appears that γ may be a good predictor of GFA for the Zr-Cu-Al alloy system, as there was a peak observed in sample 1 indicative of significant level of crystallinity in this sample while samples 2 to 5 showed broad halos indicating good GFA for these systems.

Though γ appears to correlate well with GFA for the Zr-Cu-Al system, no major change in the γ value is observable when Cu is replaced by Ni. In other words, sample 1 and 2 have almost the same γ values as sample 6 and 7. One of Inoue's three empirical rules [9] required to form a good BMG is a large difference in the enthalpy of mixing between the main three constituent elements. Since there is a significant difference in the

enthalpy of mixing of Cu in Zr (-78 KJ/mol) when compared to the enthalpy of mixing of Ni in Zr (-165 KJ/mol), a considerable difference in the value of γ should be expected for samples of similar composition but with different alloying elements (i.e. different enthalpy of mixing). However, a negligible difference in the γ value for the Zr-Cu-Al and Zr-Ni-Al means that the GFA parameter γ does not fully capture the effect of alloying elements or difference in the enthalpy of mixing on GFA for a given alloy system. [10]. In summary, Table 2 shows the complexity involved in analyzing GFA of different alloying systems. It is clear from Table 2, that the values of ΔT_x, T_{rg} and γ show conflicting trends for the Zr-Cu-Al and Zr-Ni-Al systems. This definitely means that these three indicators cannot be jointly used to analyze the GFA of different alloying systems. Also, previous claims of γ being an excellent GFA indicator do not appear to be justified because no change in γ was observed with variation in alloying elements (or enthalpy of mixing) in this study. In a later section, an additional GFA indicator will be discussed which has been shown to account for fragility in glass forming system which is consistent with enthalpy of mixing calculations.

4.3 Thermal Relaxation Study

When considering BMG's for commercial applications, it is essential to understand their behavior over an extended period of time considering the metastable nature of the system. The tendency of BMGs to relax was considered and analyzed in the current study for samples 2 and 7 by using annealing induced relaxation approach. Samples 2 and 7 were considered because they contained Cu and Ni elements, respectively.

4.3.1 Enthalpy Relaxation

For this study, the samples were heat treated as mentioned in the experimental approach. The specific heat of the samples was scanned using a DSC. After annealing, the samples were tested using the XRD technique to confirm they had not crystallized. Figs.53 and 54 shows the XRD graph for samples 2 and 7 respectively, annealed at 600 K for 18 hr. The diffraction pattern shows a broad halo with no sharp peaks confirming they are still amorphous.

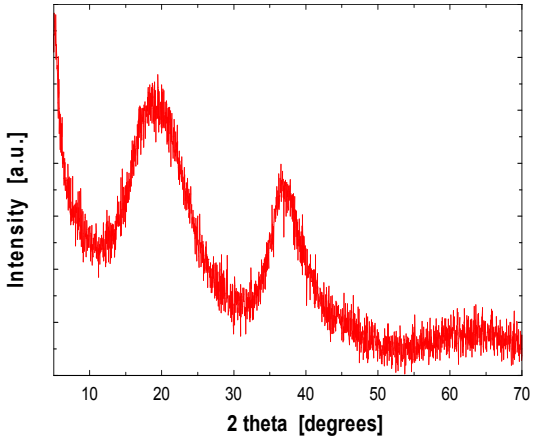

FIG.53 XRD graph of $Zr_{65}Cu_{23}Al_{12}$ annealed 600 K 18 hr (Sample 2)

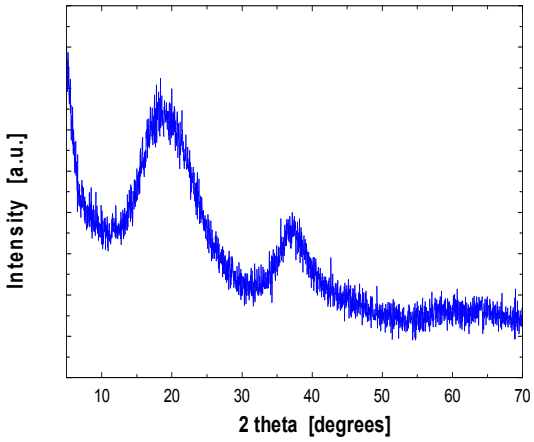

FIG.54 XRD graph of $Zr_{65}Ni_{23}Al_{12}$ annealed 600 K 18 hr (Sample 7)

The specific heat measured as a function of temperature for the as-obtained and annealed samples using DSC are illustrated in the thermographs below.

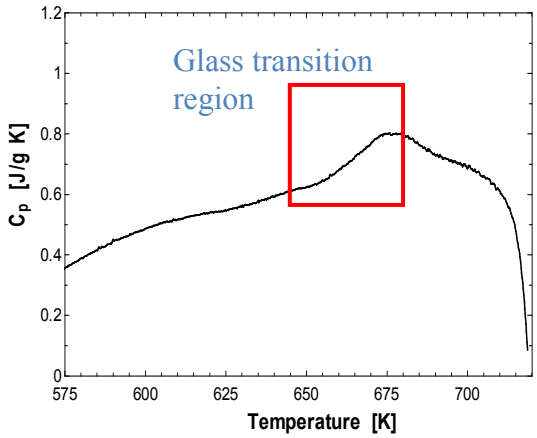

FIG.55 C_p graph of $Zr_{65}Cu_{23}Al_{12}$ as-is (Sample 2)

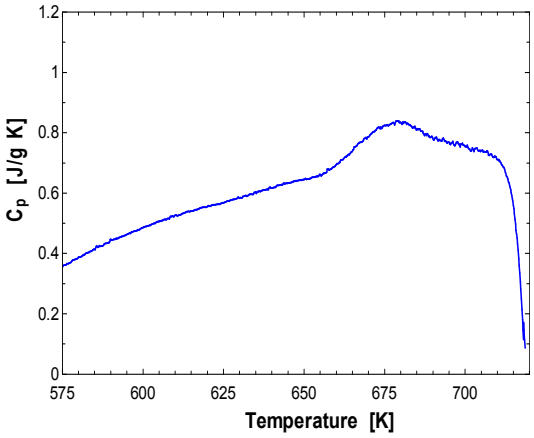

FIG.56 C_p graph of $Zr_{65}Cu_{23}Al_{12}$ annealed 600 K 0.5 hr (Sample 2)

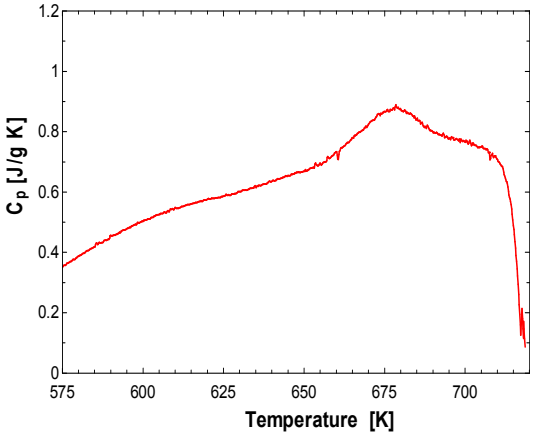

FIG.57 C_p graph of $Zr_{65}Cu_{23}Al_{12}$ annealed 600 K 2 hr (Sample 2)

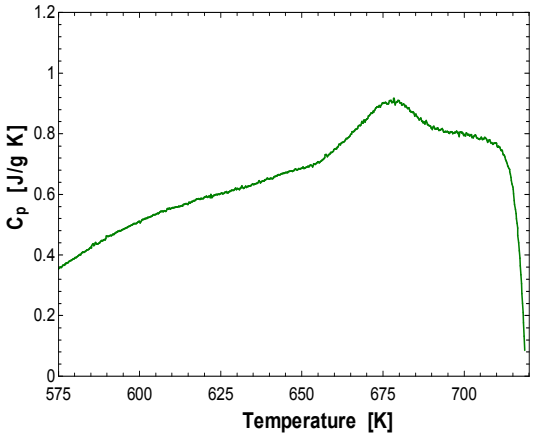

FIG.58 C_p graph of $Zr_{65}Cu_{23}Al_{12}$ annealed 600 K 4 hr (Sample 2)

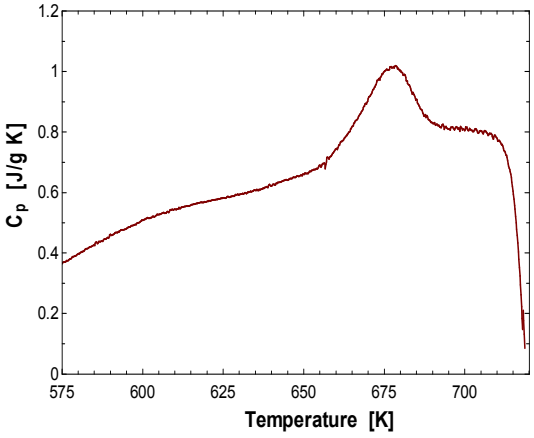

FIG.59 C_p graph of $Zr_{65}Cu_{23}Al_{12}$ annealed 600 K 10 hr (Sample 2)

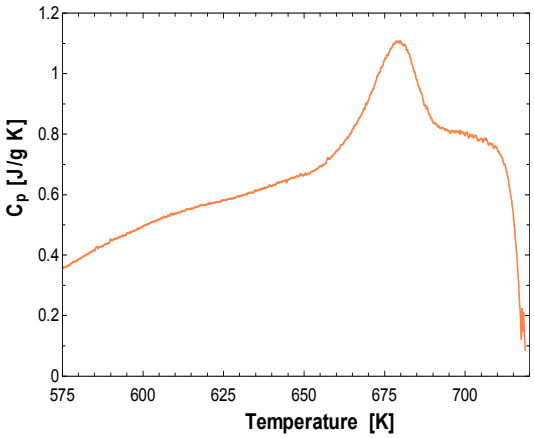

FIG.60 C_p graph of $Zr_{65}Cu_{23}Al_{12}$ annealed 600 K 18 hr (Sample 2)

Figs.55 to 60 illustrates how the specific heat of sample 2 varies with temperature for the as-obtained, and samples annealed for different periods of time below T_g. As seen in Fig.55 the specific heat of the as-obtained sample increases slowly with temperature and then rapidly in the glass transition range where it reaches a maximum value at 676 K. Beyond the glass transition, the specific heat decreases rapidly due to the onset of crystallization of the sample. Furthermore, there is no sudden change (jump) in specific heat capacity as the sample approaches glass transition. A jump in the specific heat has been observed in certain BMGs like Pd-based systems [8]. A jump in specific heat has been associated with the fragility of the liquid phase. A fragile liquid is considered to be constituted of structures that are less stable when compared to stronger liquids. As a result, specific heat jump is observed when fragile BMGs approach glass transition [8]. The absence of any jump in specific heat in the current Zr-Cu-Al system is indicative of the strong glass forming nature of the liquid

melt. The specific heat curves for the annealed samples (Figs.56 to 60) show a relative increase in the specific heat when approaching the glass transition region when compared to the as-obtained sample. This is better observed when the specific heat curves are overlaid as shown in Fig.61.

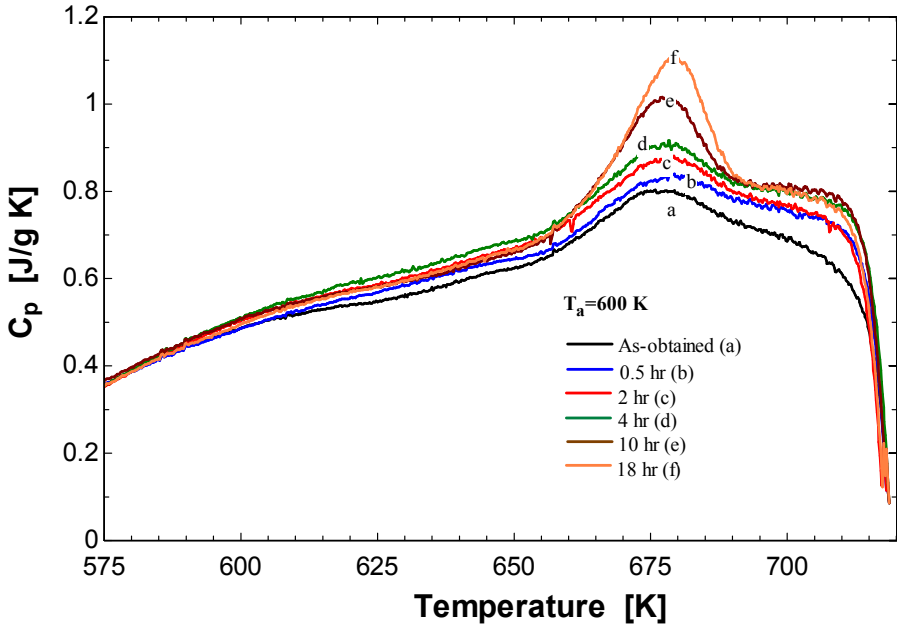

FIG.61 C_p graph of as-obtained and annealed $Zr_{65}Cu_{23}Al_{12}$ (Sample 2)

In a similar manner, the specific heat of the as-obtained and the annealed $Zr_{65}Ni_{23}Al_{12}$ samples (sample 7) were also found using DSC as shown in the thermographs in the following page. Fig.62 shows the specific heat of the as-obtained sample 7 as a function of temperature. As in sample 2, there is no jump seen in the specific heat of sample 7, confirming that Zr-based BMGs are made of strong glass forming liquids. Figs.63 to 67 shows the specific heat behavior of the annealed samples.

As seen in sample 2, the specific heat of the annealed sample 7 increases when approaching the glass transition region.

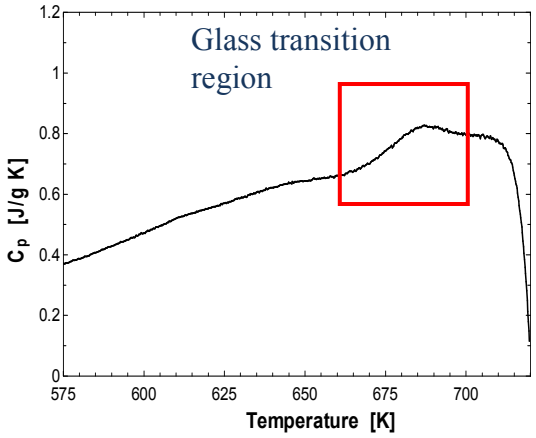

FIG.62 C_p graph of $Zr_{65}Ni_{23}Al_{12}$ as-is (Sample 7)

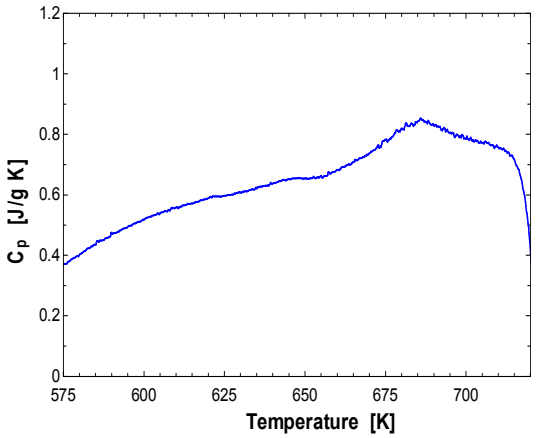

FIG.63 C_p graph of $Zr_{65}Ni_{23}Al_{12}$ annealed 600 K 0.5 hr (Sample 7)

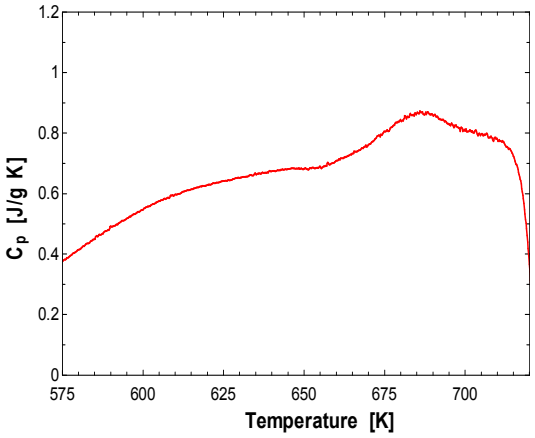

FIG.64 C_p graph of $Zr_{65}Ni_{23}Al_{12}$ annealed 600 K 2 hr (Sample 7)

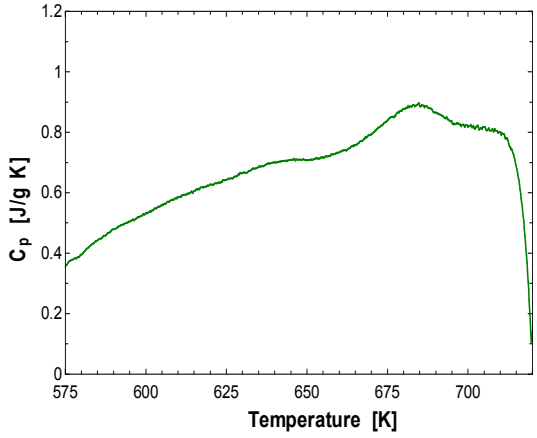

FIG.65 C_p graph of $Zr_{65}Ni_{23}Al_{12}$ annealed 600 K 4 hr (Sample 7)

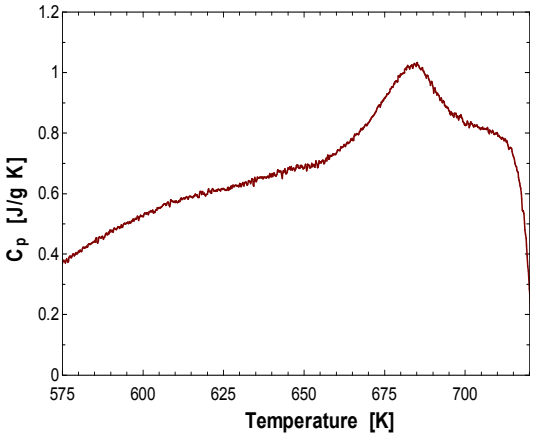

FIG.66 C_p graph of $Zr_{65}Ni_{23}Al_{12}$ annealed 600 K 10 hr (Sample 7)

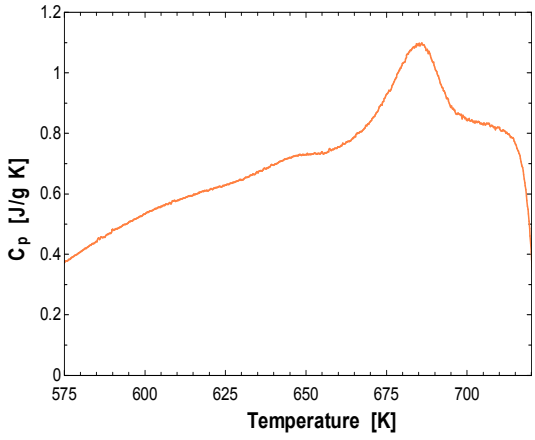

FIG.67 C_p graph of $Zr_{65}Ni_{23}Al_{12}$ annealed 600 K 10 hr (Sample 7)

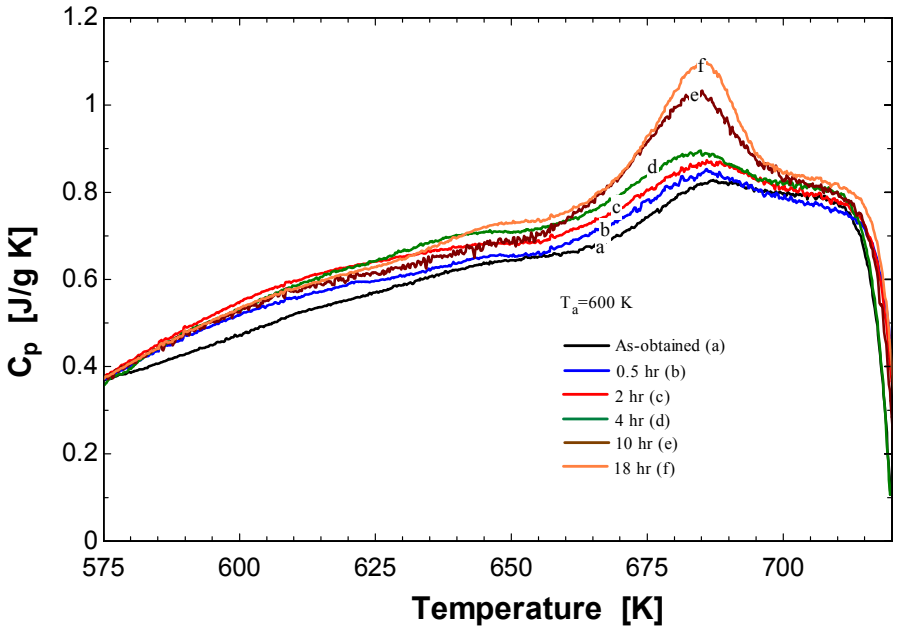

FIG.68 C_p graph of as-obtained and annealed $Zr_{65}Ni_{23}Al_{12}$ (Sample 7)

In Fig.68 the specific heat curves of the as-obtained and annealed samples are overlaid. From the figure, it is evident that the specific heat of the annealed sample tends to increase with annealing time as it approaches the glass transition temperature. This is expected in metastable systems which approach equilibrium under favorable conditions.

When BMG samples are annealed at temperatures below T_g, they tend to undergo relaxation due to their metastable nature. During relaxation, BMGs release the excess heat capacity contained in them. When annealed samples are reheated above annealing temperature, they normally recovered the heat capacity lost during annealing [36, 37]. The difference in the area enclosed between the heat curves for as-obtained sample and the annealed sample correspond to the enthalpy lost on annealing, which is the enthalpy

recovered on heating [19] beyond the annealing temperature. The recovery of the lost heat capacity seems to be due to the entropy changes experienced by the sample at higher temperature during fast heating. An increase of entropy during heating at temperatures above the annealing temperature should have prompted an increase in the heat capacity of the material, which resulted in the recovery of the lost heat capacity. This is shown with entropy calculations below. The area under each specific heat curve from the annealing temperature (600 K) to the completion of glass transition for sample 2 and sample 7 was calculated by using trapezoidal integration in Matlab. The difference in area between each annealed sample and the as-is sample was calculated, which gives the value of the enthalpy lost on annealing. The enthalpy recovered during heating was plotted as a function of annealing time and fitted with a mathematical function. The dependence of enthalpy recovery on annealing time was found to fit well into a stretched exponential relaxation function:

$$\Delta H_T(t_a) = \Delta H_T(\infty)\{1 - \exp[-(\frac{t_a}{\tau})^{\beta}]\} \quad (1)$$

where $\Delta H_T(\infty)$ is the equilibrium (asymptotic) value of $\Delta H_T(t_a)$ for $t_a \to \infty$ at the annealing temperature T_a, τ is the relaxation time constant and β is the Kohlrausch exponent that has a value between 0 and 1. The stretched exponential relaxation function has been used to estimate the amount of time a metastable system requires to reach equilibrium when subjected to annealing [22].

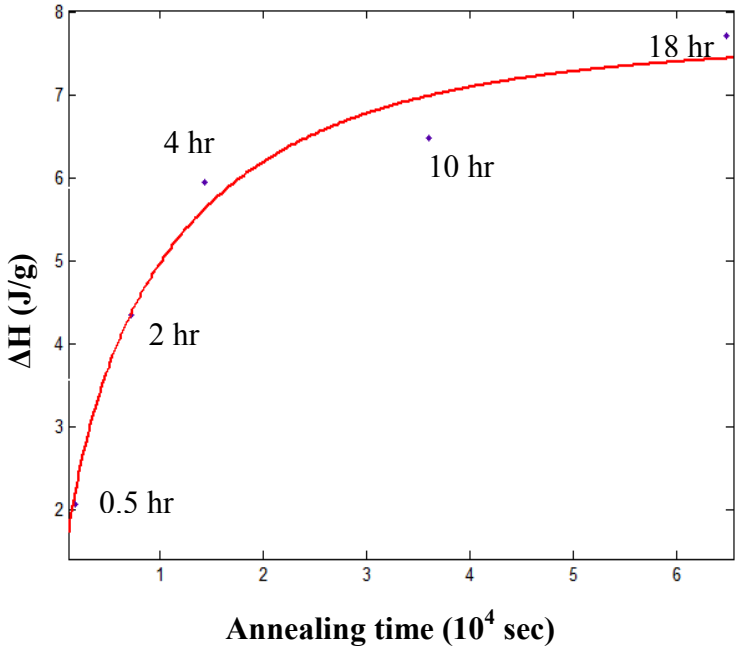

FIG.69 Recovered enthalpy as a function of annealing time $Zr_{65}Cu_{23}Al_{12}$ (Sample 2)

Figs.69 and 70 shows the enthalpy recovery plotted as a function of annealing time for sample 2 and sample 7, respectively. The enthalpy recovery rate seems to increase gradually with annealing time initially before slowing down for longer annealing time periods.

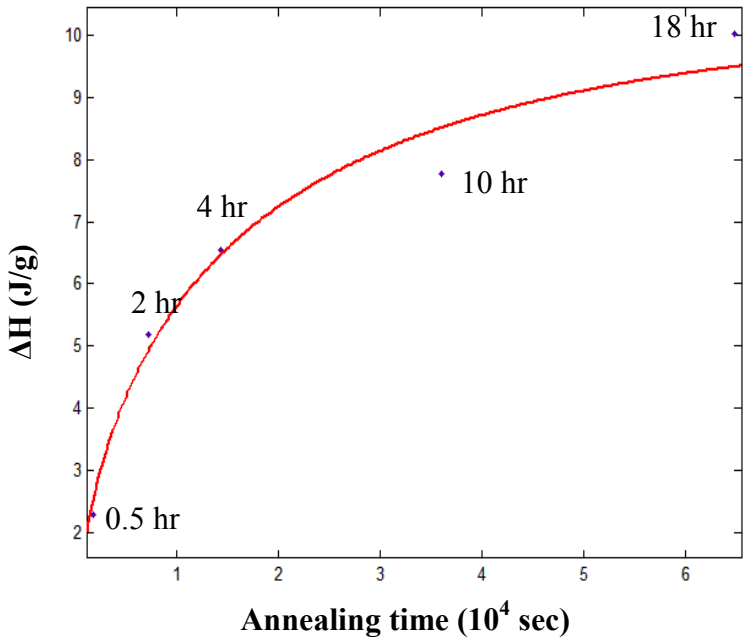

FIG.70 Recovered enthalpy as a function of annealing time $Zr_{65}Ni_{23}Al_{12}$ (Sample 7)

As shown in Figs.69 and 70 the enthalpy recovery process with annealing time fits well the stretched exponential function: $\Delta H_T(t_a) = \Delta H_T(\infty)\{1-\exp[-(\frac{t_a}{\tau})^{\beta}]\}$ as shown in Table 3. The fitting parameters for the enthalpy relaxation for sample 2 and sample 7 are shown in Table 3.

Table 3 Fitting parameters for enthalpy relaxation using a stretched exponential function

Alloy Description	**ΔH_T (∞) (J/g)**	**τ (s)**	**β**	**R^2**
$Zr_{65}Cu_{23}Al_{12}$	7.6	9299	0.66	0.976
$Zr_{65}Ni_{23}Al_{12}$	10.4	15000	0.61	0.972

From previous research [22, 38], the values for the parameters $\Delta H_T(\infty)$ and τ were found to increase with decreasing annealing temperature. This occurs because at higher temperatures the mobility of the atoms is greater and as a result, they achieve thermodynamic equilibrium faster during annealing when compared to lower annealing temperatures [22]. Furthermore, it has been found that the enthalpy relaxation time τ follows an Arrhenius behavior $\tau = \tau_0 \exp(E / k_B T)$ where τ_0 is a pre-exponential factor, k_B is the Boltzmann constant, E the activation energy and T the annealing temperature [8]. So as annealing temperature drops, the relaxation time is expected to increase exponentially making it difficult to measure it at low annealing temperatures.

From Table 3 we see that the Kohlrausch exponent β for sample 2 is 0.66, and for sample 7 is 0.61. The value of β has been observed to show strong temperature dependence and tends to increase with increasing annealing temperature. It also approaches unity when the annealing temperature is close to the glass transition temperature (T_g) [38]. In past research, the value of β has been found to be around 0.78 for La [22] and Pd-based [8] BMGs for annealing temperatures close to T_g. Considering the fact that in this study the annealing temperature (T_g - 60 K) is quite far from T_g, the value of β observed for the current Zr-based BMGs is considerably higher than the La and Pd-based BMGs.

The magnitude of β in BMGs is considered to be important because it is an indicator of how strong or fragile the liquid melt is. While for strong liquids the value of β can approach unity, fragile liquids can have a value of β as low as 0.5 [38]. From this information we can conclude that the current Zr-based BMGs are strong glass formers

on account of the high value of β found during relaxation. Furthermore, the fact that sample 2 has a slightly higher value of β when compared to sample 7 indicates that Zr-Cu- based BMGs may be stronger glass formers than Zr-Ni-based BMGs though the value of γ (0.90) was almost the same for both samples. From this finding, the author would like to state that the fragility of the liquid may be an important factor to consider other than the GFA parameters like T_{rg} and γ while trying to compare the glass forming ability of different alloy systems.

4.3.2 Entropy Relaxation

When BMGs are annealed, changes in specific heat and enthalpy values are observed. Such changes are indicative structural changes within the material. One way to understand the structural effects on annealing on BMG samples is by observing how the entropy of the system changes and how the degree of disorder decreases with relaxation. The entropy change for the as-obtained and annealed samples was calculated for sample 2 and sample 7 from the specific heat data provided above. The entropy S change of the system was calculated using the relation, $\Delta S = \int_{T1}^{T2} \frac{C_p}{T} dT$ for all the samples assuming no changes in volume. The difference in entropy between each annealed sample and the as-obtained sample was calculated and then plotted with respect to annealing time. Figs.71 and 72 show how the entropy change varies with annealing time.

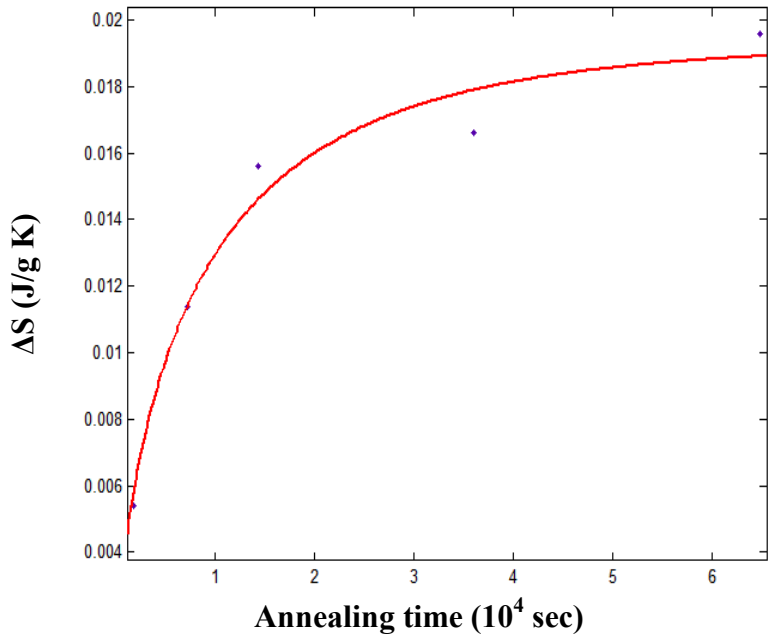

FIG.71 Entropy change as a function of annealing time $Zr_{65}Cu_{23}Al_{12}$ (Sample 2)

As seen in Figs.71 and 72, the entropy recovery on reheating can be adequately fit using stretched exponential function as a function of annealing time as follows:

$$\Delta S_T(t_a) = \Delta S_T(\infty)\{1 - \exp[-(\frac{t_a}{\tau})^{\beta_s}]\} \qquad (2)$$

where, $\Delta S_T(\infty)$ is the equilibrium (asymptotic) value of $\Delta S_T(t_a)$ for $t_a \to \infty$ at the annealing temperature T_a, τ is the relaxation time constant and β_s is the Kohlrausch exponent that has a value between 0 and 1.

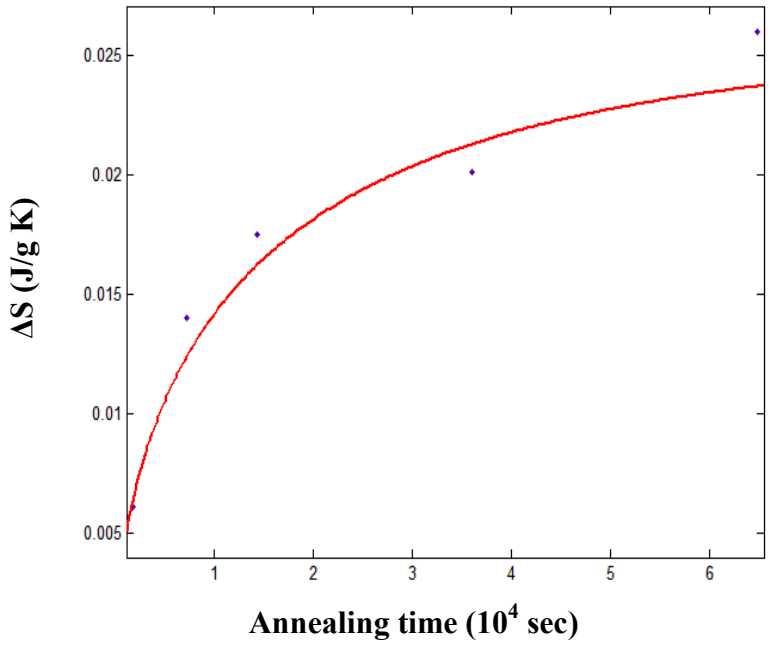

FIG.72 Entropy change as a function of annealing time $Zr_{65}Ni_{23}Al_{12}$ (Sample 7)

The stretched exponential function was used to fit the entropy data since the same function form was able to fit enthalpy changes (Equation 1) well with R^2 of over 0.97. From Equation 2, it is evident with annealing time the entropy or the level of disorder in the system decreases gradually as it reaches an equilibrium state over extended annealing periods. The fitting parameters for the stretched exponential function are shown in Table 4.

Table 4 Fitting parameters for entropy relaxation using a stretched exponential function

Alloy Description	**$\Delta S_T(\infty)$ (J/g K)**	**τ (s)**	**β_s**	**R^2**
$Zr_{65}Cu_{23}Al_{12}$	0.019	8549	0.67	0.973
$Zr_{65}Ni_{23}Al_{12}$	0.026	14770	0.61	0.949

The values for the relaxation time constant τ and Kohlrausch (entropy-based) exponent β_s in Table 4 are quite similar to the values obtained for the enthalpy relaxation parameters in Table 3, which means that most thermal properties may show a stretched exponential relaxation with time. The amount of entropy recovered through the production of entropy during re-heating (thermal activation [39]) can be used to assess the ordering effect of annealing on BMGs.

4.3.3 Activation Energy

In relaxation of BMGs, a minimum amount of energy (activation energy) is required for samples to start the relaxation process. The required activation energy for relaxation can be found using the Kissinger analysis [39, 40] and the heat flow curves. Figs.73 and 74 show the heat flow curves for samples 2 and 7 annealed at 600 K for 18h. To determine activation energy, the samples were heated at heating rates of 10, 30, 50 and 75 °C/min.

As seen in Figs.73 and 74, with an increase in the heating rate, the onset (T_g) and the peak (T_p) of the glass transition shifts to higher temperatures indicative of the kinetic nature of BMG during heating. With increasing heating rates the shift in the peaks varied between 678 K to 703 K and 684 K to 710 K for samples 2 and 7, respectively. This suggests that at higher heating rates, the samples have less time to undergo relaxation and to exhibit changes in thermal properties.

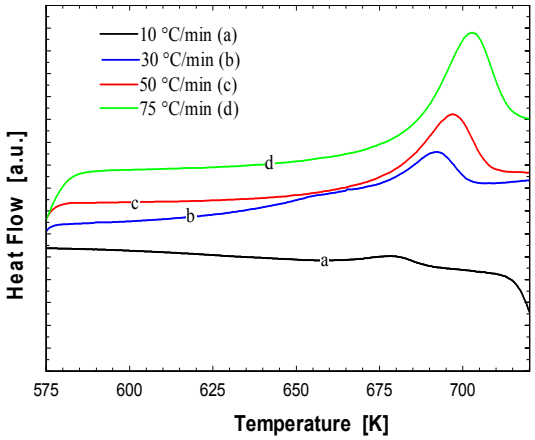

FIG.73 Influence of heating rates on glass transition peak $Zr_{65}Cu_{23}Al_{12}$ (Sample 2)

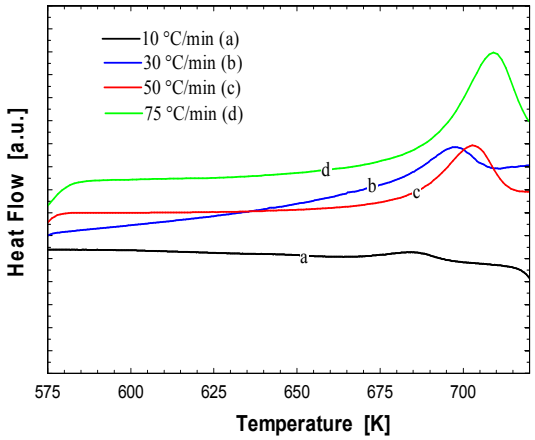

FIG.74 Influence of heating rates on glass transition peak $Zr_{65}Ni_{23}Al_{12}$ (Sample 7)

The shift in the peak (T_p) of the glass transition was used to find the activation energy of the glass transition using the Kissinger equation:

$$\ln\left(\frac{\beta_K}{T_p^2}\right) = C - \frac{E_a}{RT_p} \tag{3}$$

where β_K is the heating rate, T_p is the glass transition peak, R is the gas constant, C is a constant and E_a is the activation energy for relaxation. The activation energy was found from the Kissinger plot, which is obtained by plotting $\ln\left(\frac{\beta_K}{T_p^2}\right)$ against $\frac{1}{T_p}$. The slope of the corresponding linear fit obtained from the plot was used to find the activation energy. The Kissinger plots for sample 2 and 7 are shown in Figs.75 and 76.

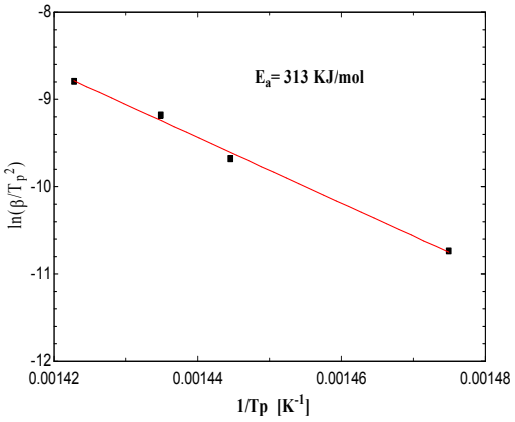

FIG.75 Kissinger Plot $Zr_{65}Cu_{23}Al_{12}$ annealed 600 K 18 hr (Sample 2)

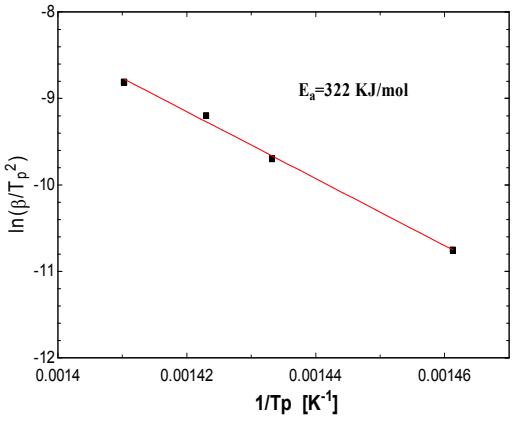

FIG.76 Kissinger Plot $Zr_{65}Ni_{23}Al_{12}$ annealed 600 K 18 hr (Sample 7)

As seen in Figs.75 and 76 the plots have a good linear relation, which is indicative of an Arrhenius temperature dependence on relaxation. The activation energy for relaxation for sample 2 and 7 were found to be 313 KJ/mol and 322 KJ/mol, respectively. In past research, the activation energy for the diffusion of small sized atoms like Ni was found to be around 200 kJ/mol, while for medium sized atoms, it was found to be around 300 kJ/mol [12]. The activation energy for the current BMGs is around 300 kJ/mol, which means that the Aluminum atoms with an atomic size of 143 pm may have diffused in the samples better. According to Vianco and Li [41], the activation energy found through Kissinger analysis is an indicator of the amount of energy required to induce an order-to-disorder transition in BMGs. Given the magnitude of activation energy in the Zr-based system, it can be concluded that the relaxed samples are relatively stable when compared to other BMGs when annealed.

4.3.4 Comparison of Thermal Properties of Amorphous and Crystalline Structures

An important aspect in the study of BMGs is to understand the difference in physical properties between the crystalline and amorphous structures of Zr-based system. As part of the study, the specific heat of the crystalline structures for samples 2 and 7 were also measured in the same temperature range as the as-obtained samples using DSC. Figs.77 and 78 show the comparison between specific heat for the as-obtained and crystalline structures of sample 2 and sample 7. As it can be observed, the specific heat of the crystalline structure is considerably lower than for the as-obtained samples because of the absence of a glass transition process in the crystalline samples.

This is a further confirmation of the metastable nature of metallic glasses because of the excess heat capacity stored in them.

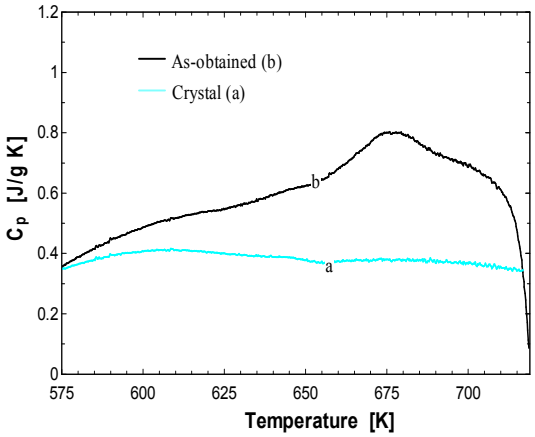

FIG.77 C_p graph of $Zr_{65}Cu_{23}Al_{12}$ as-is and crystal (Sample 2)

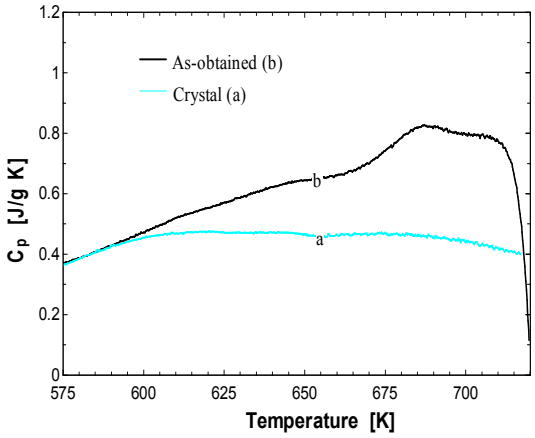

FIG.78 C_p graph of $Zr_{65}Ni_{23}Al_{12}$ as-is and crystal (Sample 7)

From the specific heat data obtained, the enthalpy and entropy differences were calculated by using the same method as the one used for the relaxed samples. The

enthalpy and entropy differences between the as-obtained (H_a, S_a) and crystal (H_c, S_c) for sample 2 and sample 7 were tabulated as shown in Table 5 below.

Table 5 Enthalpy and entropy difference between as-obtained and crystal samples

Sample No	Alloy Description	$\Delta H = (H_a - H_c)$ (J/g)	$\Delta S = (S_a - S_c)$ (J/g-K)
2	$Zr_{65}Cu_{23}Al_{12}$	22.8	0.059
7	$Zr_{65}Ni_{23}Al_{12}$	16.3	0.042

As expected, the entropy of the crystallized structure is lower than that of the amorphous structure. The excess entropy in BMGs further confirms the higher degree of disorder in metallic glasses and their tendency to move towards equilibrium by relaxation.

4.4 EXAFS Study

The purpose of the EXAFS study was to understand the effect of alloying elements, annealing temperature and annealing time on structure of the BMG samples. Samples 2 and 7 containing Cu and Ni, respectively were used in the study. The as-obtained samples and the samples annealed at 600 K for 2 hr and 18 hr were used for the study. Along with this, the crystallized samples (heated at 1073 K for 30 minutes) were also probed to understand how the amorphous and crystalline structures vary for Zr-based BMGs. Due to relatively higher thickness of the samples; it was only possible to probe the Zr-edge of the samples.

The raw XAFS spectra of the as-obtained and annealed samples of $Zr_{65}Cu_{23}Al_{12}$ (Sample 2) and $Zr_{65}Ni_{23}Al_{12}$ (Sample 7) are shown in Figs.79 and 80, respectively. The XAFS spectra of the crystallized sample and Zr-metal (used for calibration) are also shown for comparison purpose.

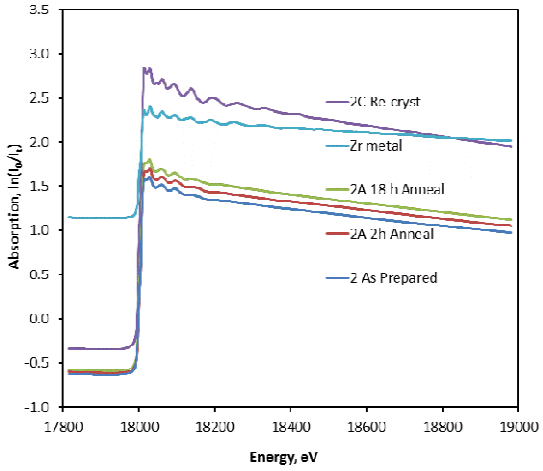

FIG.79 Raw EXAFS spectra of the as-obtained, relaxed, and crystallized samples of $Zr_{65}Cu_{23}Al_{12}$ (Sample 2)

In the case of XAFS spectra for sample 2 shown in Fig.79, the crystallized sample appears to be 25-30 % thicker than the amorphous sample based on the magnitude of absorption observed. The XAFS spectra of sample 7 shown in Fig.80 appear to have all the samples to be of comparable thickness based on the total absorption effect in these samples.

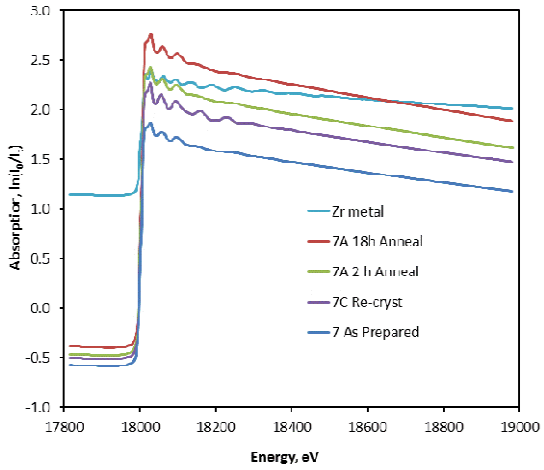

FIG.80 Raw EXAFS spectra of the as-obtained, relaxed, and crystallized samples of $Zr_{65}Ni_{23}Al_{12}$ (Sample 7)

By subtracting the background from the XANES spectrum and normalizing it, the derivative XANES spectrum is obtained. The photon energy is then converted to a photoelectron wave vector k mathematically, and this is further normally multiplied by k^2 to compensate for the attenuation of the EXAFS amplitude at high k values. The k^3 conversion ensures the weighting of the EXAFS oscillations uniformly over the k range. By applying Fourier transformation to this k^3 in the k space we obtain the radial structure function. The RSF is considered to be a one dimensional representation of the local structure around the Zr atoms. In the RSF, the position of the peaks is related to the distance between the absorber and the neighboring atoms while the size of the peaks is related to the number and types of the neighboring atom. The Figs.81 and 82 show Zr-XANES spectra and the derivative XANES spectra, the k^3 chi-spectra, and the RSF spectra derived from the XANES spectra.

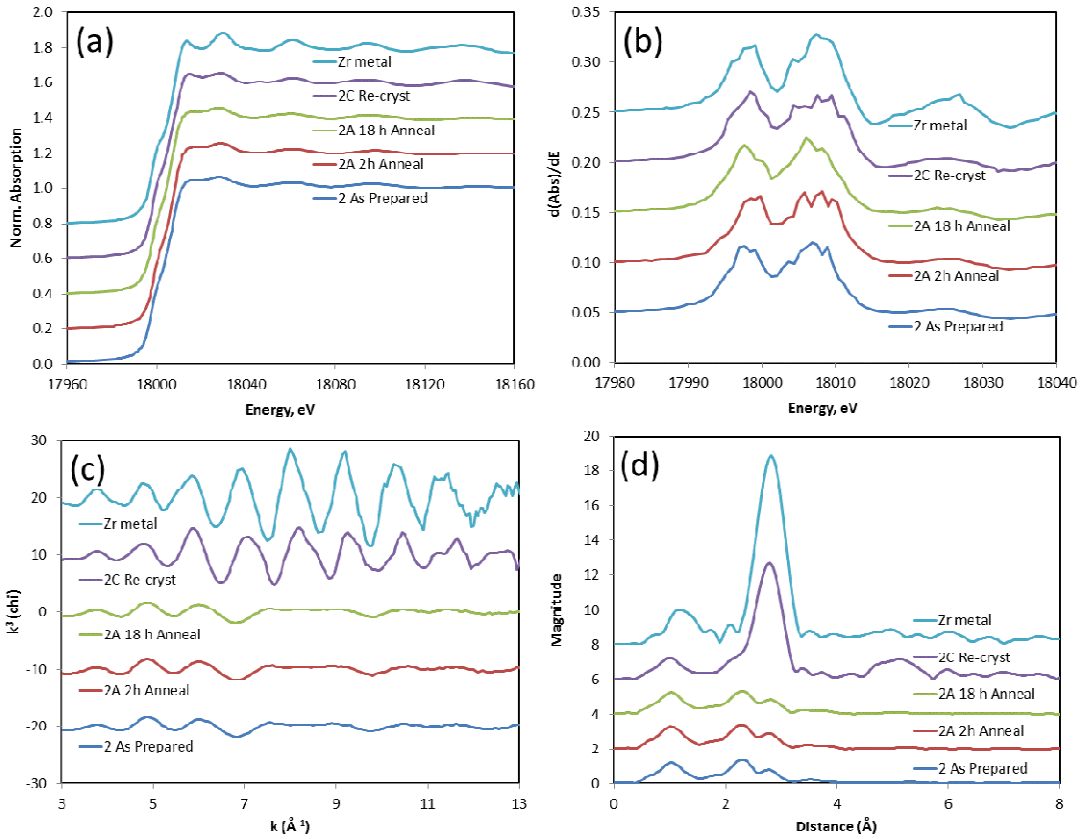

FIG.81 Zr XAFS spectra obtained from thin strips of differently treated alloys of composition $Zr_{65}Cu_{23}Al_{12}$ and from Zr metal foil; (a) XANES spectra; (b) derivative XANES spectra; (c) EXAFS (k^3chi) spectra; and (d) RSF spectra

The individual sample spectrum shown in Figs.81 and 82 has been displaced vertically arbitrarily from the one below it to compare each spectrum better. Fig.83 is an expanded view of the RSF spectra which is used to analyze differences between the as-obtained and annealed samples.

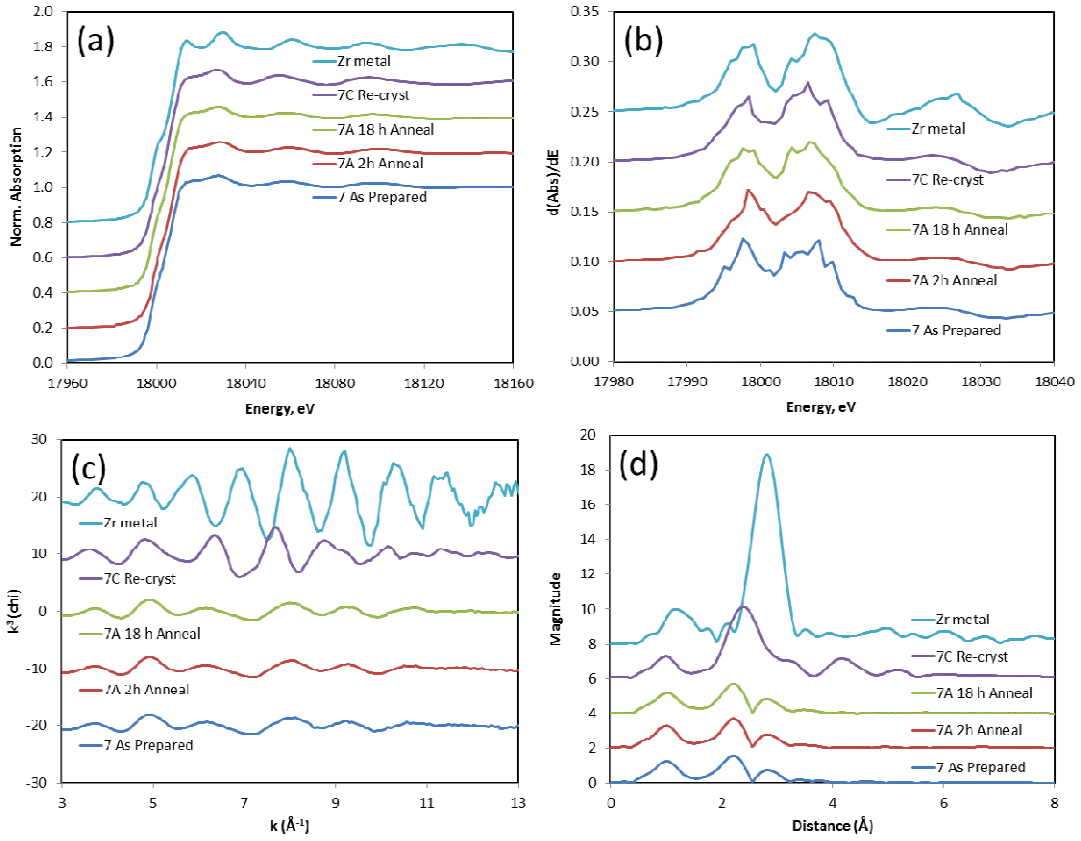

FIG.82 Zr XAFS spectra obtained from thin strips of differently treated alloys of composition $Zr_{65}Ni_{23}Al_{12}$ and from Zr metal foil; (a) XANES spectra; (b) derivative XANES spectra; (c) EXAFS (k^3chi) spectra; and (d) RSF spectra

In Figs.81 and 82, it can be seen that there are considerable differences in the spectra between the amorphous and crystallized structures. As seen in Figs.81 (c) and 82 (c) the amorphous structures have a much weaker fine structure when compared to the crystalline alloy and Zr metal.

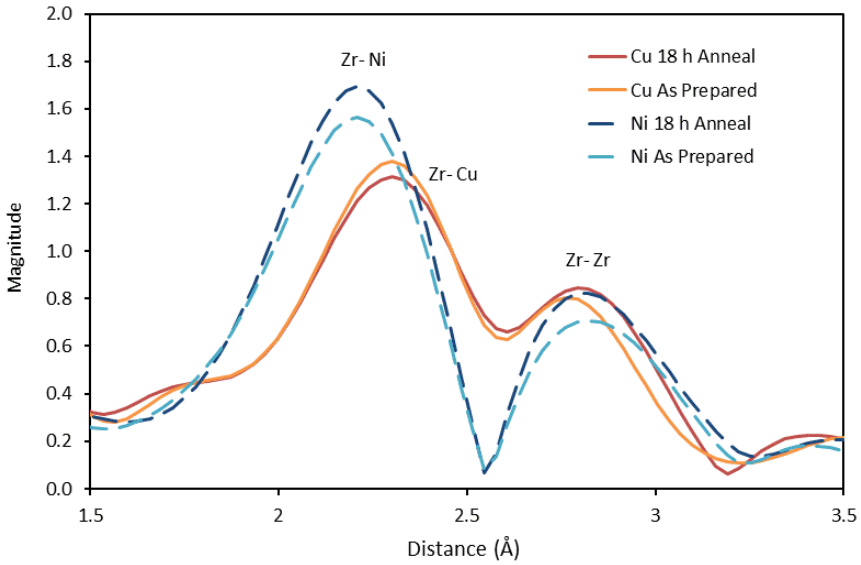

FIG.83 Expansion of RSF spectra shown in Fig.81 (d) and Fig.82 (d)

The oscillating peaks seen in Figs.81 (c) and 82 (c) (k^3chi) for the crystalline structure are due to the interference that arises from the backscattering of photoelectrons from the Zr atom being probed and its nearest neighbors. The strength of this interference is decided by the interatomic distances, coordination number and the symmetry in the arrangement of nearest neighboring atoms from the atom being probed. In the case of the crystalline structure these peaks are more pronounced because of the regular periodic arrangement of atoms in the crystals. In the amorphous and relaxed (annealed at 600 K for 2 hr and 18 hr) samples, the lack of order in the atomic arrangement is evident due to the absence of pronounced peaks.

In the RSF spectrum of the pure Zr metal as shown in Figs.81 (d) and 82(d), a major peak at about 2.75 Å is observed, which arises from the shell of 12 Zr atoms surrounding the Zr atom being probed. A similar but smaller peak is seen in the RSF

spectra for the amorphous samples 2 and 7 at the same distance, which can therefore be attributed to the Zr atoms in the vicinity of the Zr atom being probed. However, in the case of the as-obtained sample 2 and sample 7, a small but more significant peak is seen at about 2.3 Å, which can be attributed to the Cu and Ni atoms, respectively in the first coordination shell of Zr. The peak for Ni is slightly larger than the Cu peak, which suggests a slight difference in short range order in the structures.

In the crystalline Zr-Cu-Al sample, a major peak at around 2.73 Å is attributed to the Zr atoms in the first coordination shell of Zr. The number of Zr atoms surrounding the Zr atom in the Zr-Cu-Al alloy was estimated to be 11 ± 2. This suggests that metallic Zr is one possible phase in the Zr-Cu-Al crystalline sample. However, the Zr-Zr distance is about 0.03 Å less when compared to the Zr-Zr distances in pure Zr, and the Debye-Waller factor was 30 % larger indicating the structure may not be simply α-Zr (pure Zr). In the case of the Zr-Ni-Al, the peak appears to be offset from the peak of Zr metal as seen in Fig.82 (d). The offset peak is indicative of a Zr-Ni crystal phase in sample 7, which is in contrast to Zr-metal phase in sample 2 as seen in Fig.81 (d).

The spectra for the as-obtained and relaxed sample of 2 and 7, if not vertically displaced (as in Figs.81 and 82) would appear to be one single composite trace, which almost overlap over each other. This suggests that with relaxation, there is no significant change in the local environment of Zr in the samples. However, as seen in Fig.83 there are significant differences observed between the spectra of sample 2 and sample 7.

Fig.83 illustrates spectra for both samples 2 and 7 in the as-obtained and relaxed condition. The spectra shows two peak, the larger one at 2.3 Å (Zr-Cu) for sample 2, and

2.2 Å (Zr-Ni) for sample 7, and the smaller one is at around 2.75 Å (Zr-Zr). The larger peak arises from the Ni or Cu atoms in the first coordination shell, while the smaller peak arises from the Zr atoms. For sample 7, both the peaks (Zr-Ni and Zr-Zr) tend to be higher for the sample annealed for 18 hr when compared to the as-obtained sample. For sample 2, the first peak (Zr-Cu) is higher for the as-obtained sample, while the second peak (Zr-Zr) is higher for the annealed sample. From these observations, it is evident that annealing has an effect on the local structure of Zr-based alloys. From the structural relaxation studies, it appears that there are no significant changes in terms of atomic transport, interatomic distance or coordination number that occur among Zr atoms on annealing. However, the presence of alloying elements (Ni or Cu) has an effect on the local structure that results from annealing. A similar behavior has been reported for $Mg_{65}Cu_{25}Gd_{10}$ systems [42]. The other and probable reason for structural relaxation appears to be changes in free volume with annealing in the BMG samples. The free volume theory states that an atom has a tendency to move into a vacant space in its vicinity leading to relaxation movement [23]. As a result of annealing, though there is no long range atomic transport as seen in this study, there may be a reduction in the free volume of the structure that occurs by changes in interatomic distances between the atoms at the local level [43]. From previous calorimetric measurements, a relation between enthalpy change and free volume has been derived that states $\Delta H = \beta^* \Delta V_f$ where ΔH is the enthalpy change, ΔV_f is the average free volume, and β is a constant with a dimension of energy [18]. Furthermore, this relation has been proven experimentally for $Zr_{55}Cu_{30}Ni_5Al_{10}$ BMG. A similar study may be required in the future

to analyze changes in the ternary Zr-BMGs like the one used in the current study to have a better understanding of structural relaxation.

4.5 Resistance Measurements

The resistance measurements were conducted using a two point probe on samples 1 through 8, samples 2 and 7 annealed at 600 K for 2 hr and 18 hr, and the crystallized samples. The sample length was nominally 25 mm, while the width and the thickness of the samples varied. As a result of the variation in thickness and width, the values obtained can be used only for a comparative study of resistance with varying composition, alloying elements, annealing temperature and annealing time.

Table 6 Summary of resistance measurements from two point probe

Sample	Alloy Composition	Resistance (Ω)	Standard Deviation, σ
Sample 1	$Zr_{70}Cu_{16}Al_{14}$	1.86	0.09
Sample 2	$Zr_{65}Cu_{23}Al_{12}$	2.54	0.35
Sample 3	$Zr_{60}Cu_{30}Al_{10}$	2.65	0.39
Sample 4	$Zr_{55}Cu_{37}Al_{8}$	2.08	0.24
Sample 5	$Zr_{50}Cu_{46}Al_{4}$	2.02	0.39
Sample 6	$Zr_{70}Ni_{16}Al_{14}$	1.99	0.35
Sample 7	$Zr_{65}Ni_{23}Al_{12}$	2.59	0.32
Sample 8	$Zr_{50}Ni_{46}Al_{4}$	2.11	0.32
Sample 2 600 K 2 hr	$Zr_{65}Cu_{23}Al_{12}$	2.20	0.40
Sample 2 600 K 18 hr	$Zr_{65}Cu_{23}Al_{12}$	2.03	0.14
Sample 2 Crystal	$Zr_{65}Cu_{23}Al_{12}$	1.28	0.09
Sample 7 600 K 2 hr	$Zr_{65}Ni_{23}Al_{12}$	2.30	0.11
Sample 7 600 K 18 hr	$Zr_{65}Ni_{23}Al_{12}$	1.95	0.23
Sample 7 Crystal	$Zr_{65}Ni_{23}Al_{12}$	1.15	0.01

Three measurements were taken for each sample and the average of the measurements was calculated. The average resistance for each sample and the standard deviation in measurements are summarized in Table 6.

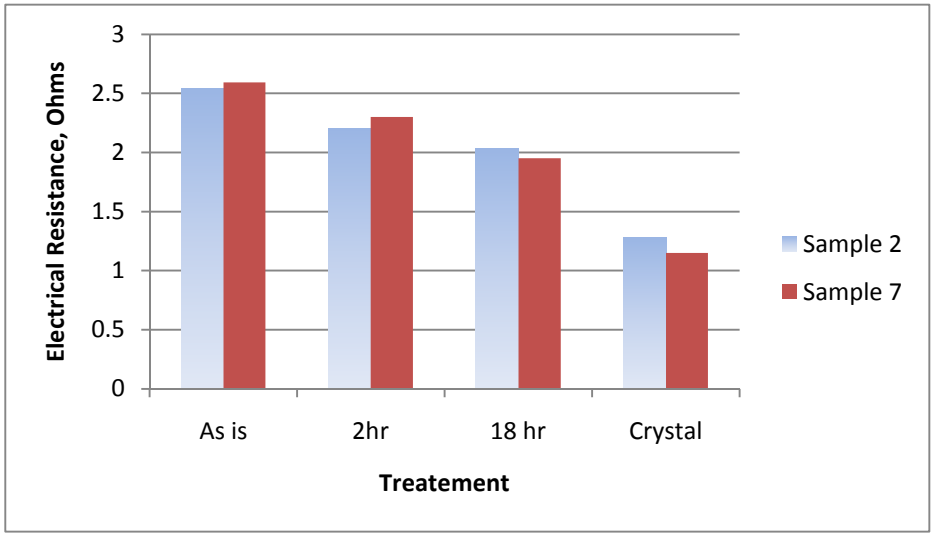

FIG.84 Comparison of electrical resistance variations with annealing

While there is no clear trend observable within different compositions of Zr-Cu-Al and Zr-Ni-Al compositions, it is seen that the resistance of Zr-Ni-Al samples is more than that of the Zr-Cu-Al samples for the same composition. This can be explained to be due to the higher electrical conductivity of Cu when compared to Ni.

The resistance of the relaxed samples 2 and 7 (annealed at 600 K for 2 hr and 18 hr) is lesser than the as-obtained samples. Furthermore, the resistance of samples annealed for 18 hr is less than the resistance of the samples annealed for 2 hr as seen in Fig.84. These observations suggest that with annealing, there are minor variations that

occur in the structure of the samples in the short range order that leads to a higher electrical conductivity in the samples [44, 45]. The resistance of the crystallized samples was found to be lesser than the as-obtained and relaxed samples. This can be explained to be a result of long range order developing on crystallization in these samples, which therefore have an improved electrical conductivity than the amorphous samples.

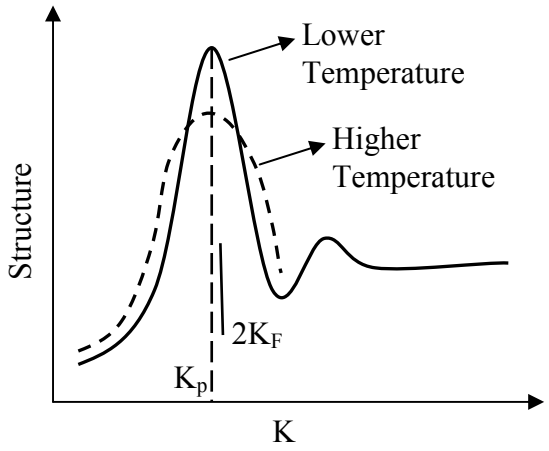

FIG.85 Variation of structure factor with annealing [46]

The explanation for the decrease in resistance described above is based on the atomic arrangements in the samples. However, this decrease in resistance may be interpreted better by the Ziman theory. Metallic glasses are believed to be made of randomly distributed ions and conductive electrons at the atomic level. The ions are randomly distributed throughout space and their arrangement can be described as a pair correlation function which can be measured experimentally by X-ray or neutron scattering. By applying a Fourier transform to the pair correlation function, the structure

factor can be obtained. The main peak in the structure factor represents the nearest neighbor distance of the ions in space which is called K_p. The conduction electrons tend to form a free-electron cloud with a spherical Fermi surface. The diameter of this Fermi sphere is called the Fermi wave number denoted as k_F [30]. A negative temperature coefficient of resistance is found to be characteristic of alloy systems where K_p is approximately equal to $2k_F$ according to Ziman theory. When BMGs are annealed, it is believed that the main peak in the structure factor decreases in height (K_p), and broadens due to the increased disorder. With a decrease in $K_{p,}$ it tends to approach $2k_{F,}$ hence the resistance drops [46] as shown in Fig.85. This may explain the resistance of the relaxed samples being lower than the as-obtained samples in the current Zr-based BMGs.

CHAPTER V

CONCLUSIONS

This chapter presents the conclusions drawn from the results obtained from GFA, thermal and structural relaxation studies and resistance measurements. Additionally, recommendations for future work in this area are provided.

5.1 Glass Forming Ability

- The Zr-Ni-Al alloys were found to have a higher supercooled liquid (ΔT_x) region when compared to Zr-Cu-Al alloys of same compositions.

- The γ value for Zr-Cu-Al alloys was found to increase with decreasing Zr content. The BMG $Zr_{50}Cu_{46}Al_4$ (Sample 5) has the best GFA (based on γ) while $Zr_{70}Cu_{16}Al_{14}$ (Sample 1) has the lowest GFA in the Zr-Cu-Al alloys. There were no specific trends found in the case of Zr-Ni-Al alloys.

- The effect of alloying elements (Cu & Ni) was not captured by γ alone. Furthermore, the GFA parameters ΔT_x, T_{rg}, and γ showed conflicting trends for the Zr-Cu-Al and Zr-Ni-Al BMGs. Thus claims that γ is an excellent GFA indicator does not appear to be justified through this current study. Fragility (β) was found to be a better GFA indicator.

5.2 Thermal Relaxation

- The specific heat of the annealed samples showed a relative increase when approaching the glass transition region when compared to the as-obtained

sample. The dependence of enthalpy and entropy recovering on annealing time for $Zr_{65}Cu_{23}Al_{12}$ and $Zr_{65}Ni_{23}Al_{12}$ was found to fit well into a stretched exponential function.

- The stretching exponent β considered to be an indicator of the fragility of the liquid melt was found to be high for the current Zr-based glass indicating they are strong glass formers. Furthermore, β was found to be higher for $Zr_{65}Cu_{23}Al_{12}$ (Sample 2) when compared to $Zr_{65}Ni_{23}Al_{12}$ (Sample 7). The fragility parameter of BMG systems in the form of β may be a good GFA indicator than the other well known GFA indicators.

- The activation energy for relaxation of $Zr_{65}Cu_{23}Al_{12}$ and $Zr_{65}Ni_{23}Al_{12}$ was found to be comparable to the activation energy required for the diffusion of medium-sized atoms, which is Al in the current BMGs. Therefore, relaxation in these systems may be occurring by the short range diffusion of Al atoms.

5.3 EXAFS Studies

- The RSF spectrum of $Zr_{65}Ni_{23}Al_{12}$ (sample 7) as-obtained showed a slightly larger peak for the Zr-Ni phase when compared to the Zr-Cu phase in $Zr_{65}Cu_{23}Al_{12}$ (Sample 2) suggesting different short range order for the systems.

- The RSF spectrum for the crystallized $Zr_{65}Cu_{23}Al_{12}$ (Sample 2) showed metallic Zr being a possible separate phase, while for $Zr_{65}Ni_{23}Al_{12}$ (Sample 7), Zr-Ni phase was found to be formed after crystallization.

- With relaxation, the RSF spectrum showed different peak trends for $Zr_{65}Cu_{23}Al_{12}$ and $Zr_{65}Ni_{23}Al_{12}$ alloys indicating that alloying elements have an effect on the structural relaxation process in BMGs.

5.4 Resistance Measurements

- The electrical resistance of Zr-Ni-Al alloys was found to be higher than Zr-Cu-Al alloys of similar composition.

- The electrical resistance of the relaxed Zr-Cu-Al and Zr-Ni-Al alloys was found to be lower than the as-obtained samples. The likely causes for the reduced electrical resistance after relaxation include short range ordering or a shift in K_p as it approaches 2 K_F as described by the Ziman theory.

5.5 Recommendation for Future Work

Based on the current work, it is clear that γ is not the most reliable GFA indicator for different alloy systems. A new indicator that combines γ and fragility (β) of the melt should be developed act as a more effective GFA indicator.

There were no major variations found in the local environment of Zr with relaxation of the BMGs. The local environment around the other alloying elements Ni, Cu and Al should be studied by EXAFS or other techniques to obtain a better understanding of the effects of alloying elements and annealing time on the structural relaxation of BMGs. Density variations for the as-obtained and relaxed BMGs should also be studied to find out whether the free volume theory can be used to explain thermal relaxation in Zr-based ternary BMGs.

The resistance measurements should be conducted with a four-point probe with samples of uniform dimensions to have a better understanding of the effects of annealing and alloying elements on the variation of resistivity in BMGs.

REFERENCES

[1] Battezzati L, Castellero A, Rizzi P. Journal of Non-Crystalline Solids 2007;353:3318.

[2] Feltz A. Amorphous inorganic materials and glasses. Von A. Feltz VCH Verlagsgesellschaft. New York , Weinheim/VCH Publishers, 1993.

[3] Mattern N. Journal of Non-Crystalline Solids 2007;353:1723.

[4] Budhani R, Goel T, Chopra K. Bulletin of Materials Science 1982;4:549.

[5] Kumar G, Tang HX, Schroers J. Nature 2009;457:868.

[6] Nascimento MLF, Souza LA, Ferreira EB, Zanotto ED. Journal of Non-Crystalline Solids 2005;351:3296.

[7] Poon SJ, Shiflet GJ, Guo FQ, Ponnambalam V. Journal of Non-Crystalline Solids 2003;317:1.

[8] Fan GJ, Löffler JF, Wunderlich RK, Fecht HJ. Acta Materialia 2004;52:667.

[9] Senkov ON, Scott JM. Scripta Materialia 2004;50:449.

[10] Miller PLM. Bulk metallic glasses. New York, Springer Verlag, 2008.

[11] Turnbull D. Contemporary Physics 1969;10:473.

[12] Isabella G, Minalben BS, Ralf B. Acta Materialia 2007;55:1367.

[13] Lu ZP, Liu CT. Acta Materialia 2002;50:3501.

[14] Lück R, Jiang Q, Predel B. Journal of Non-Crystalline Solids 1990;117-118:911.

[15] Debenedetti PG, Stillinger FH. Nature 2001;410:259.

[16] Wen P, Zhao Z, Wang W. Science in China Series G: Physics Mechanics and Astronomy 2008;51:356.

[17] Hay JN. Pure & Appl. Chem. 1995;67:1855.

[18] Zhang Y, Hahn H. Journal of Non-Crystalline Solids 2009;355:2616.

[19] Johari GP, Shim JG. Journal of Non-Crystalline Solids 2000;261:52.

[20] Chen HS, Inoue A, Masumoto T. Journal of Materials Science 1985;20:2417.

[21] Haruyama O, Nakayama Y, Wada R, Tokunaga H, Okada J, Ishikawa T, Yokoyama Y. 2010;58:1829.

[22] Zhang T, Ye F, Wang YL, Lin JP. Metallurgical and Materials Transactions A 2008;39:1953.

[23] Binder WKK. Glassy materials and disordered solids. Hackensack, World Scientific Publishing Co. Pte. Ltd, 2005.

[24] Dmowski W, Fan C, Morrison ML, Liaw PK, Egami T. Materials Science and Engineering: A 2007;471:125.

[25] Yavari AR, Moulec AL, Inoue A, Nishiyama N, Lupu N, Matsubara E, Botta WJ, Vaughan G, Michiel MD, Kvick A. Acta Materialia 2005;53:1611.

[26] Li G, Cai Q, Li H, Zheng L, He B, Sun T. Journal of Wuhan University of Technology--Materials Science Edition 2009;24:210.

[27] Concustell A, Alcalá G, Mato S, Woodcock TG, Gebert A, Eckert J, Baró MD. Intermetallics 2005;13:1214.

[28] Liebermann HH. Rapidly solidified alloys. New York, Marcel Dekker, Inc., 1993.

[29] Kokmeijer E, Huizer E, Thijsse BJ, van den Beukel A. Materials Science and Engineering 1988;97:505.

[30] Bai HY, Tong CZ, Zheng P. Journal of Applied Physics 2004;95:1269.

[31] Park ES, Lim HK, Kim WT, Kim DH. Journal of Non-Crystalline Solids 2002;298:15.

[32] Wang W-H, Wei Q, Bai HY. Applied Physics Letters 1997;71:58.

[33] Xu D, Duan G, Johnson WL. Physical Review Letters 2004;92:245504.

[34] Inoue A, Katsuya A. The Japan Institute of Metals 1996;37:1332.

[35] Zhang T, Inoue A. The Japan Institute of Metals 1999;40:301.

[36] Aji DPB, Wen P, Johari GP. Journal of Non-Crystalline Solids 2007;353:3796.

[37] Inoue A, Tsai AP, Kimura HM, Masumoto T. Journal of Materials Science 1988;23:429.

[38] Gallino I, Shah MB, Busch R. Journal of Alloys and Compounds 2007;434-435:141.

[39] Mao M, He Y. Physica Status Solidi (a) 1988;105:325.

[40] Noh TH, Inoue A, Fujimori H, Masumoto T, Kang IK. Journal of Non-Crystalline Solids 1989;110:190.

[41] Vianco PT, Li JCM. Journal of Non-Crystalline Solids 1989;107:225.

[42] Li G, Cai Q, Li H, Zheng L, He B, Sun T. Journal of Wuhan University of Technology--Materials Science Edition 2009;24:210.

[43] Ishii A, Iwase A, Fukumoto Y, Yokoyama Y, Konno TJ, Hori F. Journal of Alloys and Compounds 2010;504:S230.

[44] Wang WM, Niu YC, Wang F, Liang JC, Jin SF, Zhang WG, Bian XF. Journal of Non-Crystalline Solids 2008;354:3612.

[45] Komatsu T, Yokota R, Shindo T, Matusita K. Journal of Non-Crystalline Solids 1984;65:63.

[46] Guntherodt HJ,Kunzi HU. Metallic glasses. Ohio, American Society for Metals, 1976.

APPENDIX A

FEFF ANALYSIS FOR EXAFS DATA

(a) FEFF analysis of Zr in metallic zirconium and crystalline Zr-Cu-Al sample:

FEFF parameters were derived from the crystal structure of the zirconium metal foil using the program TKAtoms and least-squares fitting of the k^3chi spectrum using the program SixPack. The data obtained was then applied to estimate the number of Zr atoms and the Zr-Zr distance in the first coordination shell in the crystalline Zr-Cu-Al alloy sample. The results obtained from the fitting for Zr metal and the Zr-Cu-Al alloys are summarized in Table A1, Fig. A1 and Fig. A2 below.

Table A1. Results from FEFF analysis of the first coordination shell in metallic Zr and the crystalline Zr-Cu-Al sample.

Sample	Mode (range)	S_0^2	CN	E_0	R, Å	ó^2, Å^2	R_{factor}
Zr metal	R (2 – 3.4 Å)	0.08	(12)	-5.7	3.199	0.0094	0.0180
	q (3 – 13 Å^{-1})	0.08	(12)	-5.3	3.202	0.0095	0.0115
	Errors (q)	±0.01		±1.3	±0.008	±0.0009	
Zr-Cu-Al alloy crystalline	R (2 – 3.4 Å)	(0.08)	11	-7.0	3.15	0.0127	0.0454
	q (3 – 13 Å^{-1})	(0.08)	11	-6.9	3.15	0.0123	0.0329
	Errors (q)		±2	±2.1	±0.013	±0.0017	

Values in parentheses were fixed during the least-squares fitting.

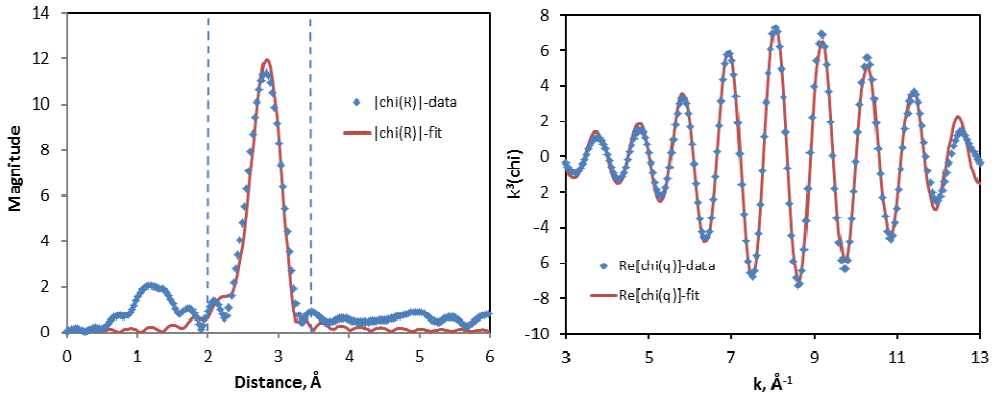

Fig. A1. FEFF least-squares fitting of the major coordination shell in metallic zirconium. Left: Fit in R-space, over the range 2 – 3.4 Å. Right: Fit to the back-transform of the isolated Zr-Zr shell (q-mode).

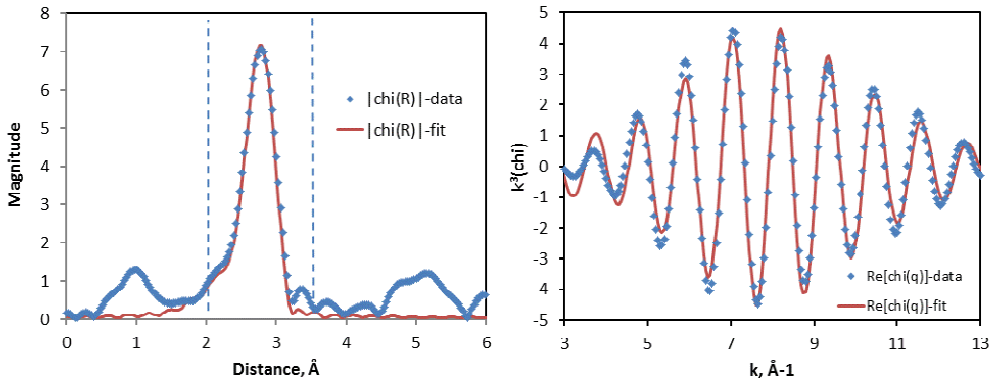

Fig. A2. FEFF least-squares fitting of the major coordination shell in the crystalline Zr-Cu-Al sample. Left: Fit in R-space, over the range 2 – 3.4 Å. Right: Fit to the back-transform of the isolated Zr-Zr shell (q-mode).

VITA

Name: Aravind Miyar Kamath

Address: Department of Engineering Technology and Industrial Distribution

MS 3367

Texas A&M University

College Station, Texas 77843-3367

Email: maravindkamath@gmail.com

Education: B.E., Mechanical Engineering, Manipal Institute of Technology,

Manipal, India, 2003

M.S., Mechanical Engineering, Texas A&M University, 2011